Layer 5 lateral entorhinal cortex neurons encode updating of object-place associations

Short title: LEC L5 neurons update object-place associations

Banks PJ[1,2,*] & Barker GRI[1,2], Booth CA[1], Kinnavane L[1], Warburton EC[1,3] & Bashir ZI[1,3*]

[1]School of Physiology, Pharmacology and Neuroscience, University of Bristol, Biomedical Sciences Building, University Walk, Bristol BS8 1TD, United Kingdom

[2,3]These authors contributed equally to the study

*Correspondence: paul.banks@bristol.ac.uk; z.i.bashir@bristol.ac.uk

Number of pages: 53

Number figures: 4 main, 2 supplementary

Number of tables: 7 main, 2 supplementary

Word counts: abstract 150, introduction 650, discussion 1023

Conflict of Interests

The authors declare no competing interests.

Acknowledgements

This work was supported by a Wellcome Trust Joint Investigator Award to E.C.W. and Z.I.B. (206401/Z/17/Z), a BBSRC project grant to Z.I.B., E.C.W and P.J.B. (BB/X000915/1) and a BBSRC project grant to E.C.W and G.R.I.B. (BB/Y006402/1). We thank Dr Emma Cahill for helpful comments on the manuscript.

Abstract

Associative recognition memory is essential for everyday life, forming cognitive representations of and recalling relationships between things we encounter and their environments. Object-place associations are represented in the lateral entorhinal and medial prefrontal cortices, however the identity of neurons in which these associations are formed, the cellular mechanisms supporting them, and how these representations react to change are not understood. Here we labelled associative recognition memory engrams, finding that engram neuron reactivation by memory recall correlated with behavioural performance only in the dorsolateral subregion of entorhinal cortex, where reactivation was overrepresented in layer 5/6. Electrophysiology from e*x vivo* slices prepared directly following memory recall revealed increased excitability in layer 5 lateral entorhinal cortex engram cells, which only occurred when engram-specific objects were reconfigured. These data identify deep layer lateral entorhinal cortex neurons as key loci of object-place associations and proposes a plastic mechanism by which pre-existing neural representations are updated.

Significance statement

Associative recognition memory is key to our normal everyday lives, but how these memories are updated and which neurons support these memories remain poorly understood. We identify a population of neurons in the deep-layers of lateral entorhinal cortex which are activated by memory encoding and whose reactivation is correlated with, and necessary for, memory retrieval, thus identifying them as engram neurons. These entorhinal neurons demonstrate increased firing following presentation of familiar cues in a novel configuration, revealing a mechanism for integrating new information into existing memories. By identifying a specific cell type and plasticity process underlying memory updating, this work advances understanding of how flexible object-place representations are maintained in the brain.

Introduction

Associative recognition memory, remembrance for objects and their associated locations and contexts, is fundamental to everyday decision making and behaviour. These memories depend on a highly interconnected brain network including the hippocampus, thalamus, perirhinal cortex (PRH), medial prefrontal cortex (mPFC) and medial and lateral entorhinal cortex (MEC, LEC; Aggleton and Nelson, 2020). Of these cortical regions, PRH has a well-established role encoding object identity and novelty, whilst mPFC performs integration of object identity, location and time (Ennaceur et al., 1997; Barker et al., 2007). The role of LEC, however, is less clear.

Classical models (Eichenbaum et al., 2007) propose that LEC is part of a processing stream representing object features and identity, which converges with spatial information from MEC to form object-context representations in the hippocampus. Emerging evidence however suggests that LEC neurons can represent dimensions not only of object identity but also of context, time and space (Deshmukh and Knierim, 2011; Deshmukh et al., 2012; Keene et al., 2016; Tsao et al., 2018; Wang et al., 2018; Nilssen et al., 2019; Wang et al., 2020; Wang et al., 2024). Indeed, lesion or inactivation of LEC impairs object-in-place (OiP) and object-in-context (OiC) memory whilst sparing simple novel object recognition (Van Cauter et al., 2013; Wilson et al., 2013; Chao et al., 2016; Kinnavane et al., 2025; though see: Vandrey et al., 2020).

Which neurons in these association cortices are prominently active during OiP memory and the plastic changes which may support memory is unclear; both superficial and deep LEC neurons have been shown to encode multi-dimensional object representations (Deshmukh and Knierim, 2011; Deshmukh et al., 2012; Keene et al., 2016). Optogenetic inhibition (Kinnavane et al., 2025) of mPFC→LEC synapses, which innervate deep layers of LEC (Kinnavane and Banks, 2022; Kinnavane et al., 2025), impairs both OiP and OiC memory whilst LEC layer 2a fan cells are crucial for associative learning (Lee et al., 2021) and object-context-place discrimination

(Vandrey et al., 2020). For mPFC, immediate-early gene studies have shown activation of mPFC by associative recognition memory tasks, but have not examined laminar activation in detail (Barbosa et al., 2013), and layer specific *in vivo* recordings are lacking.

In this study, to identify key cell populations involved in associative memory processing, we used *Fos*$^{2A\text{-}iCreERT2}$ (TRAP2; Allen et al., 2017) mice to label putative OiP memory engram cells, focussing on association cortices. OiP produced robust TRAP2 labelling at memory encoding and Fos activation following retrieval. TRAP2 and Fos double-positive neurons (engram cells which had been reactivated by retrieval) were significantly more numerous in OiP mice compared to controls, however this reactivation correlated with memory performance only in dorsal subregions of LEC. Chemogenetic inactivation showed LEC TRAP2 cells to be necessary for expression of OiP memory recall. In *ex vivo* LEC brain slices prepared from mice which had recently performed memory retrieval, layer 5 (L5) pyramidal TRAP2 neurons showed increased excitability and firing compared to unlabelled neurons; these changes were not found in other cortical engram populations and only occurred when objects were presented in a reconfigured arrangement. These data suggest a key role for LEC L5 neurons in forming object-place associations and demonstrate an engram cell specific form of plasticity related to retrieval and integration of new information into existing object-place representations.

Methods

Animals

All animal procedures were conducted in accordance with the United Kingdom Animals (Scientific Procedures) Act (1986) under project licence number PP7058522 and were approved by the University of Bristol Ethical Review Committee. The following strains of mice were used: TRAP2 (Fos$^{2A\text{-}iCreERT2}$): Fos$^{tm2.1(icre/ERT2)Luo}$/J, JAX stock 030323 generated by L.Luo (Allen et al., 2017); Ai14 (: B6.Cg-Gt(ROSA)26Sor$^{tm14(CAG\text{-}tdTomato)Hze}$/J, JAX stock 007914 generated by H.Zeng (Madisen et al., 2010)); hM4Di-DREADD (R26-LSL-Gi-DREADD): B6.129-Gt(ROSA)26Sor$^{tm1(CAG\text{-}CHRM4*,\text{-}}$

100 $^{mCitrine)Ute}$/J, JAX stock 026219 generated by B.Roth and U.Hochgeschwender (Zhu et al., 2016).
101 Mice were maintained on a reverse 12 h:12 h light:dark cycle (lights on 20:00-08:00) at constant
102 temperature and humidity with *ad libitum* food and water. Home cage enrichment was present
103 in the form of a cylindrical cardboard tube and a cellulose half-dome. Both male and female
104 mice (sex determined by visual inspection of gonads by the animal breeding unit) were used at
105 ≥10 weeks old. Mice were group housed in cages of 2-4 except for experiments involving
106 cannulated hM4Di-DREADD mice which were single housed to prevent chewing of cannulae
107 between cage-mates – for this reason, only male mice were used for these experiments due to
108 increased tolerance of single housing(Davies, 2025).

109 **Surgery**

110 Implantation of bilateral cannulae into LEC was performed under isoflurane general
111 anaesthesia (3% induction, 2-3% maintenance) and secured in a stereotaxic frame using a
112 mouse anaesthesia head holder and non-rupture ear bars (World Precision Instruments; WPI).
113 Ophthalmic ointment was applied to the eyes to prevent drying, the scalp was sterilised with 4%
114 chlorhexidine, and lidocaine (2%, 0.05 ml) was injected subcutaneously to provide local
115 anaesthesia. A scalpel incision was made along the midline of the scalp and craniotomies were
116 performed with a microdrill (WPI) and 0.5 mm burrs (Fine Science Tools). Guide cannula (26G,
117 P1Technologies, Cat#C315GAS-5/SPC) were implanted into LEC (AP -3.0mm, ML ±4.2mm, DV -
118 3.2mm relative to bregma) and secured with gentamycin bone cement (DePuy international).
119 The scalp incision was closed with surgical sutures and wound powder applied to the site. Mice
120 were given 0.5 ml subcutaneous glucose saline for hydration. Analgesia was provided via: 1.5 µg
121 intramuscular buprenorphine given at the end of surgery and 0.15 mg meloxicam given orally in
122 a palatable solution of condensed milk 24 h prior- and 24 and 48 h post-surgery. Mice were
123 allowed to recover for 2 weeks before undergoing behavioural procedures.

124 **Behavioural Procedures**

Habituation

Mice were habituated to the entire experimental regimen except objects for at least 6 days prior to activity-dependent labelling. All translocation of mice between cages and behavioural apparatus was done using cardboard enrichment tubes (Davies et al., 2022). Mice were first transported from the home room to the behavioural room within 2 hours of dark phase onset where they would remain for a similar duration and timing to activity-dependent labelling day. Cage mates were split into individual experimental cages which had the same dimensions, bedding and enrichment as their home cages, and placed in a designated position in a storage rack surrounded by black curtains. Mice were allowed to individually explore the empty arena for 10 min per day of habituation. This was followed by ~3-5 min of handling in a neighbouring room for habituation to injection procedures. TRAP2 x hM4Di-DREADD mice received additional habituation to intracerebral infusions in the form of daily handling and a dummy infusion of saline 7 days prior to activity-dependent labelling. Following habituation procedures mice remained in their experimental cages in the storage rack for at least 3 hours before being returned to their home cages with cage mates.

Apparatus

Behavioural testing took place in a wooden, open-topped arena (50 cm x 50 cm) with three black and one grey 40 cm high walls, positioned within a sheet-aluminium faraday cage. The floor was covered with sawdust for all experiments. Behaviour was monitored using an overhead digital camera. Objects of approximately 8 x 8 x 8 cm were constructed from Lego (Lego UK) and varied in colour and shape. The bases of the objects were secured to the arena floor using Velcro and covered with sawdust.

Object-in-place behavioural testing

148 Lego objects were placed in the four corners of the arena ~ 10 cm from the walls. In the sample
149 phase mice were released into the centre of the arena from their cardboard enrichment tube
150 and allowed to explore objects for 10 min. Mice were returned to their experimental cage for a 5
151 min delay period during which all objects were cleaned with 100% ethanol to remove olfactory
152 cues. Objects were then replaced into the arena with either the left- or right-hand objects
153 exchanging position - starting positions and the side on which objects were reconfigured were
154 counterbalanced between mice. Mice were then returned to the arena for 10 min (test phase 1)
155 and the time spent exploring objects in novel positions was compared to exploration of objects
156 which remained static. Either 7 days or 48h after test phase 1, mice underwent test phase 2 (10
157 min). Objects were placed in the arena, objects which had switched location in test phase 1
158 remained stationary while the objects which had been stationary in test phase 1 now switched
159 locations (Fig. 1A). Familiar arena mice underwent the identical procedure without objects in
160 the arena.

161 *Activity-dependent neuronal labelling*

162 Immediately following behavioural procedures, mice were taken to the injection room, scruffed
163 and injected intraperitoneally with 50 $mg.kg^{-1}$ 4-hydroxytamoxifen (4-OHT; 70% Z-isomer; Hello
164 Bio Cat#HB6040). TRAP2 x hM4Di-DREADD mice were briefly anaesthetised with isoflurane
165 before intraperitoneal injection of 4-OHT to allow replacement of dummy cannulae (P1
166 technologies, Cat#C315DCS-5/SPC). 4-OHT was dissolved in 100% ethanol (10 $mg.ml^{-1}$) at 37°C
167 for 30 min (briefly vortexed at ~5 min intervals), then diluted 1:2 with a 1:4 mixture of
168 castor:sunflower seed oils (Sigma). The ethanol was evaporated off using a vacuum centrifuge
169 and the resulting 10 $mg.ml^{-1}$ 4-OHT solution used for injection. Mice were immediately returned
170 to their experimental cage following injection and kept in darkness for a minimum of 3 h before
171 being put back into home cages with cage mates and being returned to the home room. Vehicle

172 injected animals received an injection of the castor:sunflower oil mixture at an equivalent
173 volume to what would have been administered if they were injected with 4-OHT.

174 *Chemogenetic silencing of LEC engram neurons*

175 Following activity dependent labelling of OiP neurons, TRAP2 x hM4Di-DREADD mice were given
176 a period of 48 h to allow expression of hM4Di protein; 48 h was chosen to attempt to restrict
177 protein expression to neuronal somata and thus permit inhibition of only LEC engram neurons,
178 whereas at longer delays hM4Di might be expected to accumulate in the presynaptic input to
179 LEC neurons (Stachniak et al., 2014). Following the 48 h delay, mice received intracerebral
180 infusions of Clozapine-N-oxide (CNO; Hello Bio Cat#HB6149) or vehicle into LEC (internal
181 cannula, P1 technologies Cat#C315LIS-5/SPC). General infusion procedures were performed
182 as described previously(Barker et al., 2006). CNO was dissolved at 30 μM in sterile saline and
183 0.05% DMSO and infused at a volume of 0.5 μl per site, over a 2 min period. Vehicle infusions
184 consisted of sterile saline and 0.05% DMSO. 15 min after the start of infusion, mice were
185 returned to the behavioural apparatus for 10 min for test phase 2 in which the object pair which
186 had been static at test phase 1 exchanged position, whilst those which had been re-arranged in
187 test phase 1 now remained static (i.e., if the left hand objects had been moved at test phase 1,
188 the right hand objects were moved at test phase 2).

189 **Immunofluorescence staining**

190 Ninety minutes after the start of test phase 2 mice were given an overdose of sodium
191 pentobarbital (20 mg, Euthatal, Rhone Merieux) and then transcardially perfused with 0.1 M
192 phosphate buffer (PB) followed by 4% paraformaldehyde in 0.1 M PB. Brains were removed and
193 post-fixed in 4% paraformaldehyde for 2h and then incubated in 30% sucrose in PB at room
194 temperature overnight. Brains were sectioned in the coronal plain into 40 μm sections with a
195 cryostat. Four serial sets of sections were collected for each brain region of interest and stored
196 in cryopreserve before immunofluorescent staining. Before immunostaining commenced

197 sections were washed 5 times (2 x 30 min at RT, 3 x 10 min at 35°C) in phosphate buffered saline
198 (PBS) to remove cryopreserve. Sections then underwent staining for Fos and tdTomato. Sections
199 were incubated in 1% H_2O_2 in PBS for 30 min and then washed three times in PBS. Sections
200 underwent antigen retrieval by incubating in sodium citrate buffer (10 mM, pH 6.0) at 80°C for 30
201 min. When sections had cooled down to RT they were washed four times in 0.2% Triton-X 100 in
202 0.1 M PBS (PBST). Sections were then incubated in mouse-on-mouse blocking buffer (Vector
203 laboratories Cat#MKB-2213, 2 drops per 2.5 ml) in PBST for 1 h followed by incubation in
204 blocking buffer (5% normal goat serum and 2.5% bovine serum albumin in PBST) for 1 h.
205 Sections were then incubated in primary antibody solution to Fos (1:1000 mouse anti-Fos; Hello
206 Bio, Cat#HB8006) and tdTomato (1:1000 chicken anti-mCherry; Abcam, Cat#ab205402) in
207 blocking buffer for 48 h at 4°C. Sections were washed 4 times in PBST and then incubated in
208 secondary antibody solution (1:250 goat-anti mouse Alexa Fluor 488 conjugate (Invitrogen
209 Cat#A-11029) and 1:500 goat anti-chicken Alexa Fluor 594 conjugate (Abcam Cat#ab150176) in
210 blocking buffer) for 24 h at 4°C. Sections were washed four times in PBST and then mounted
211 onto polylysine coated slides. Sections were dried for 24 h in the dark and then coverslipped
212 using Vectashield with DAPI (Vector Laboratories, Cat#H-1500).

213 **Electrophysiological analysis of engram TRAP2 cell excitability**

214 48 h after activity dependent labelling of TRAP2-Ai14 mice, mice underwent test phase 2 (except
215 Fig. 4A). Mice were then transported to a slicing room in their experimental cage covered with a
216 black plastic bag and acute *ex vivo* brain slices were prepared. Approximately 10 minutes
217 elapsed between the end of test 2 and the onset of slice preparation.

218 *Acute slice preparation*

219 Mice were anaesthetised with isoflurane (3%) and tested for absence of hind paw pain reflex
220 and eye-blink reflex before decapitation. The brain was rapidly dissected and placed into a
221 beaker of ice-cold sucrose (in mM: 189 sucrose, 26 $NaHCO_3$, 10 D-glucose, 5 $MgSO_4$, 3 KCl, 1.25

222 NaH_2PO_4, 0.2 $CaCl_2$; Fisher Scientific) bubbled with 95% O_2/5% CO_2. The cerebellum was
223 removed with a scalpel and a coronal cut was made at the approximate rostro-caudal level of
224 the thalamus. The brain was affixed to the tissue stage of a vibratome (7000smz-2, Campden
225 Instruments) with cyanoacrylate glue. 300 µm thick coronal brain slices were made and placed
226 in artificial cerebrospinal fluid (aCSF; in mM: 124 NaCl, 26 $NaHCO_3$, 10 D-glucose, 3 KCl, 2
227 $CaCl_2$, 1.25 NaH_2PO_4, 1 $MgSO_4$) bubbled with 95% O_2/5% CO_2. Slices were incubated for 1 hr at
228 34°C and then subsequently at room temperature until use. Recordings began 1 hr after slicing.

229 *Electrophysiological recording*

230 Coronal slices were placed into a submerged recording chamber perfused with 34°C aCSF at a
231 rate of 2ml.min^{-1} and immobilised using a slice anchor (Warner Instruments). Anterior-posterior
232 depth was determined using a brain atlas (Paxinos and Franklin, 2019) under a 4x objective and
233 wide field oblique infra-red optics. Neurons were imaged using a 40x immersion objective and
234 oblique infra-red and fluorescence imaging. tdTom neurons were matched with neighbouring
235 unlabelled neurons with similar morphology in the same layer and region of the slice, typically
236 30-100 µm from each other. Recordings were acquired using either simultaneous dual whole-
237 cell patch clamp or sequential single cell recordings. LEC and perirhinal cortex cellular location
238 was determined using a brain atlas (Paxinos and Franklin, 2019); L5 neurons were 125-300 µm
239 from the white matter, fan cells were in L2a which was visible as a dense cell layer adjacent to
240 the almost acellular region in L1 which extended ~100 µm from the pial surface (Vandrey et al.,
241 2020). mPFC L2/3 and L5 were defined as 125-325 µm and 325-650 µm from the pial surface of
242 PrL, respectively (Anastasiades et al., 2019).

243 Whole-cell current-clamp recordings were made using borosilicate glass micropipettes (3–6
244 MΩ; Harvard Apparatus, Cat# GC150-10F,) filled with potassium gluconate intracellular solution
245 (in mM: 125 K-gluconate, 40 HEPES, 2 NaCl, 2 MgATP, 0.3 NaGTP, 0.2 EGTA, 0.25% Biocytin, 290-
246 300 mOsm). Series resistance was 10-30 MΩ and was not compensated. Data was obtained

247 with a Multiclamp 700A amplifier (Molecular Devices), digitized at 40 kHz (National Instruments
248 USB-6341) and low-pass filtered at 4 kHz using WinLTP3.00 software (Anderson and
249 Collingridge, 2007).

250 Resting membrane potential (RMP) was recorded immediately after break-in. Subsequently,
251 constant-current was applied to keep cells at approximately -70 mV. Liquid junction potential
252 was calculated to be 16.4 mV using LJPCalc and was not corrected. To assess subthreshold
253 membrane properties and firing properties, cells were injected with a series of 500 ms square
254 wave pulses ranging from -100 to +300 pA. To determine rheobase, cells were injected with an
255 800 ms linear current ramp to an amplitude sufficient to elicit at least one action potential. To
256 evoke afterdepolarisation potentials (ADP), cells were injected with a 1-2 ms duration square
257 current of 1000-4000 pA amplitude such that a single action potential was evoked. To evoke
258 AHP, neurons were injected with 10 current pulses (1-2 ms duration, 1000-4000 pA amplitude)
259 at 50 Hz. Cells were held for ~15 min in the whole cell configuration before slow withdrawal of
260 the recording electrode to pull an outside-out patch to aid biocytin reconstruction. The location
261 of neurons with respect to each other was recorded to assist in identifying biocytin stained
262 neurons.

263 *Immunohistochemical biocytin staining*

264 Following recording, slices were fixed in 4% paraformaldehyde in 0.1 M PB overnight and
265 subsequently stored in 0.1 M PB until staining. Slices were washed 6 x 10 min in PB, then
266 incubated in 3% H_2O_2 in PB for 30 min to block endogenous peroxidase activity, then washed
267 again as above before incubation in 1% (vol/vol) avidin–biotinylated HRP complex (ABC; Vector
268 Laboratories Cat#PK-6100) in PB containing 0.1% (vol/vol) Triton X-100 at RT for 3 hrs. Slices
269 were then washed as above before incubation in 3,3'-diaminobenzidine solution (Sigma,
270 Cat#D4418-50SET) for 5-10 min until staining of neuronal structures was visible. The reaction
271 was stopped by transferring slices to cold PB, followed by further washing as above. Slices were

272 mounted, coverslipped using Mowiol 4-88 mounting media (Sigma, Cat#81381) and allowed to
273 dry overnight before imaging.

274 *Exclusion and classification criteria*

275 Biocytin-immunohistochemistry was used to make post-hoc corrections to cell location (layer,
276 subregion) and morphology where neurons had been mis-labelled at the time of recording.
277 Pyramidal neurons had primary apical dendrites projecting towards the pia mater, whilst L2 fan
278 cells had a characteristic broad dendritic arbor extending into L1 (Tahvildari and Alonso, 2005;
279 Vandrey et al., 2020). Neurons were excluded from analysis if their RMP exceeded -50 mV,
280 membrane potential became persistently unstable or series resistance exceeded 30 MΩ.
281 Individual electrophysiological sweeps were excluded where membrane potential was
282 transiently unstable, deviated from -70 mV, or spontaneous activity prevented accurate
283 measurement of data.

284 **Quantification and statistical analysis**

285 *Behaviour scoring and statistics*

286 Exploratory behaviour was manually scored and defined as the animal directing its nose
287 towards the object at a distance <2 cm and actively exploring the object. Any other behaviour,
288 such as looking around while sitting on or resting against the object, grooming within 2 cm of an
289 object, or digging at object bases, was not considered object exploration. Discrimination
290 between the objects was calculated using a discrimination ratio (DR), calculated as the
291 absolute difference in the time spent exploring the moved and unmoved stimuli divided by the
292 time spent exploring all the objects. The DR takes into account individual differences in the total
293 amount of object exploration (Ennaceur and Delacour, 1988; Dix and Aggleton, 1999). For the
294 combined DR the exploration of the moved stimuli in test phase one and two was added
295 together and the same was done for the unmoved stimuli and these combined values were used

296 to calculate the combined DR. Performance in each test phase and for the combined DR was
297 assessed using a two-tailed one-sample t-test against chance (DR = 0). Exploration across the
298 phases of the task were compared using a one-way within subjects ANOVA. Post-hoc
299 comparisons used a Bonferroni correction. For chemogenetic silencing of engram cells in LEC,
300 DR and total object exploration levels across test phase 1 and 2 was compared using a two-way
301 ANOVA with drug as a between subjects factor and test phase as a within subjects factor. Post-
302 hoc comparisons examined simple main effects. Comparison of exploration in the sample
303 phase used a one-way between subjects ANOVA. Performance in the test phases was assessed
304 against chance using a one-sample t-test as previously described.

305 *Cell counting protocol and statistics*

306 For the quantification of tdTom, Fos and DAPI expression in mPFC, LEC and PRH, cells were
307 counted bilaterally from 4 (mPFC) or 5 (LEC and PRH) coronal sections from specific locations
308 along the anterior-posterior length of each brain region (Table 1). Fluorescent images were
309 acquired using a Leica Microsystems DM6 B microscope and Hamamatsu C13400-20CU Digital
310 CMOS camera via the Leica Application Suite X software using 100x magnification. Manual cell
311 counting was performed using ImageJ software. Images were split into individual channels. For
312 each cortical area, a region of interest (ROI; 0.5 mm height by 0.25 mm width) was placed over
313 layer 2/3 and layer 5/6 using the DAPI channel in each slice. Cortical regions were identified
314 using a brain atlas (Paxinos and Franklin, 2019). Cell counts for each channel were obtained as
315 follows; background subtraction was applied to remove background noise, thresholds were set
316 and images were converted to binary. The analyse particles tool was used to quantify the
317 number of labelled cells in each ROI based on particle size (50-500 μm^2 tdTom, 20-150 μm^2 Fos)
318 and circularity (0.4-1.0). Overlap between tdTom and Fos expression was determined by digitally
319 merging the analysed images for each ROI to form a composite image and the number of co-

labelled cells quantified. All cell counting was performed by an experimenter blind to the behavioural condition of each animal.

To analyse each brain subregion, cell counts in L2/3 and L5/6 ROIs were combined for each hemisphere, the counts for each hemisphere and for each AP depth counted were averaged. To generate counts for all of mPFC and LEC, the counts for the individual subregions were averaged in each animal to generate counts for the whole brain region. To generate counts for L2/3 and L5/6 of cortex, counts in each region were averaged across hemispheres and sections. These averaged counts were then converted into counts per mm^2. Percent overlap was calculated as ($tdTom^+Fos^+$ cells/$tdTom^+$ cells) * 100.

Comparisons of cell counts across the whole cortical regions between behavioural conditions used a one-way ANOVA with behavioural condition as a between subject factor. Comparison of layer 2/3 and layer 5/6 counts between behavioural conditions used a two-way ANOVA with cortical depth as a within-subjects factor and behavioural condition as a between-subjects factor. Post-hoc tests analysed simple main effects where appropriate. To analyse the relationship between memory performance and cell reactivation a Pearson's correlation coefficient was calculated comparing combined DR and % reactivation. All statistical analyses were performed using SPSS and significance was set at $p < 0.05$.

Electrophysiology statistics

Electrophysiological data were imported into MATLAB for analysis using custom-written scripts based upon Kerrigan et al. 2014 (code available on request). Action potential parameters are measured from the first action potential from the smallest square-wave current-injection which yielded an action potential. Reported input resistance values are steady-state input resistance. Statistical analysis of all electrophysiological variables was performed in GraphPad Prism 10 using Mann Whitney U test, except action potential firing where a mixed-effect model with a Greenhouse-Geisser correction applied and labelling and current injection as factors was used,

345 and ADP presence where a Chi-squared test was used. Cells were considered the experimental
346 unit for electrophysiology.

347

348

349 **Results**

350 **OiP memory performance correlates with reactivation of dorsolateral entorhinal cortex**
351 **engram cells**

352 TRAP2 mice were crossed with tdTomato (tdTom) Cre reporter *Ai14* mice (Madisen et al., 2010)
353 resulting in Fos-driven, 4-hydroxytamoxifen (4-OHT)-dependent tdTom labelling. Whilst
354 rewarding and aversive experiences produce high levels of labelling and reactivation at recall in
355 TRAP mice (DeNardo et al., 2019; Bobadilla et al., 2020), it is unknown whether every day,
356 spontaneous learning behaviours such as associative recognition memory are processed in the
357 same manner. TRAP2-Ai14 littermates were assigned to one of two experimental groups: OiP or
358 familiar arena (FA), the latter of which served as the control group (Fig. 1A). Mice assigned to the
359 OiP group preferentially explored reconfigured objects when tested at 5 min and 7 d,
360 demonstrating intact memory (Fig. S1A).

361 We focussed our analysis of TRAP2 cell activation and reactivation on two cortical regions
362 known to be essential for associative recognition memory: LEC (Wilson et al., 2013; Vandrey et
363 al., 2020; Tozzi et al., 2024; Kinnavane et al., 2025) and mPFC (Preston and Eichenbaum, 2013;
364 Barker et al., 2017). Mice which had not received 4-OHT showed negligible tdTom labelling (Fig.
365 S1B). Analysis of cell activation patterns across the whole of mPFC and LEC (Fig. 1B) revealed
366 the number of tdTom labelled cells was not significantly different between the OiP and FA
367 conditions in either brain region (Fig. 1B, Table S1). However, the number of Fos immunostained
368 cells following recall at 7 d was significantly higher in OiP compared to FA mice and, critically,

369 the percentage of Fos-immunostained tdTom cells (indicating reactivation) was significantly
370 higher in the OiP condition compared to FA in both brain regions (Fig. 1C, Table S1). These same
371 patterns of activation and reactivation were also seen when mPFC was separated into prelimbic
372 (PrL) and infralimbic cortex (IL) subdivisions and the LEC into dorsal lateral (DLent), dorsal
373 intermediate (DIent) and ventral intermediate (VIent) subdivisions (Fig. 1D; S1C, Table S1).

374 To investigate the relationship between memory performance in the OiP task and engram cell
375 reactivation, a Pearson correlation coefficient was computed for each brain region. No
376 significant correlation was found between the combined discrimination ratio (DR) and tdTom
377 cell reactivation in mPFC, nor the PrL and IL subdivisions (Fig. 1E, S1D). Analysis of LEC showed
378 a non-significant trend towards positive correlation between memory performance and tdTom
379 cell reactivation (Fig. 1E). Interestingly, analysis of LEC subdivisions identified a statistically
380 significant positive correlation in DLent, a positive but not statistically significant correlation in
381 DIent and a non-significant negative relationship in VIent (Fig. 1E). DLent may, therefore, be a
382 critical region for OiP memory retrieval.

383 The superficial and deep layers of LEC are anatomically distinct, with layers 2 & 3 (L2/3)
384 providing input into the hippocampus while layers 5 & 6 (L5/6) receive inputs from the
385 hippocampus and project to non-hippocampal regions (Ohara et al., 2021). In the whole LEC
386 significantly more tdTom cells were found in L2/3 than L5/6 in both the FA and OiP conditions,
387 whereas memory retrieval produced equal amounts of Fos labelling in L2/3 and L5/6 in both
388 behavioural tasks (Fig. 1G). Surprisingly, a significantly higher proportion of deep layer LEC
389 tdTom cells were reactivated by retrieval in both behavioural conditions (Fig. 1G). Analysis of
390 LEC subdivisions showed that this activation and reactivation pattern was consistent across all
391 three LEC subdivisions (Fig. 1G, S2A,B, Table S2), with the exception of there being no difference
392 in tdTom labelling in different layers of DLent of OiP mice (Fig. 1G, Table S2) or in the reactivation
393 of VIent layers in OiP mice (Fig. S2B, Table S2).

394 Layer analysis of mPFC as a whole did not reveal any differences in labelling between L2/3 and
395 L5/6 (Fig. S2C). In PrL, significantly more tdTom cells were found in L2/3 in both behavioural
396 tasks, however there was no significant difference in Fos labelling or reactivation between
397 layers following memory retrieval (Fig. S2D). In IL significantly more tdTom cells were activated
398 in L5/6 in the OiP task, however no significant differences in layer were observed for Fos
399 labelling or reactivation following memory retrieval for either behavioural condition (Fig. S2E,
400 Table S2).

401 In summary these data show that OiP recall robustly reactivates LEC and mPFC neurons which
402 were activated at encoding, that reactivation of LEC neurons correlates with memory
403 performance with a dorsoventral gradient, and that reactivation is highest in L5/6 LEC neurons,
404 putatively identifying deep layer DLent as a key locus of object-place representations. We next
405 determined the necessity of LEC TRAP2 neurons for memory performance.

406 **Inactivation of LEC TRAP2 cells impairs OiP memory recall**

407 If activity-labelled neurons are to be considered engram cells, in addition to their reactivation by
408 stimuli relevant to the labelling experience, their activity should also be necessary for retrieval
409 of the memory (Tanaka et al., 2014). To test this hypothesis, TRAP2 mice were crossed with Cre-
410 dependent *hM4Di-DREADD* mice to permit chemogenetic inactivation of activated neurons (Fig.
411 2A). Guide cannulae were implanted bilaterally in LEC (Fig. 2B), targeting DLent where TRAP2
412 cell reactivation was significantly correlated with memory performance (Fig. 1F). Following
413 recovery from surgery, mice underwent OiP testing before injection with 4-OHT to drive
414 expression of hM4Di in active neurons (Fig. 2A). We then assessed the effect of hM4Di-mediated
415 inactivation on memory retrieval by infusing vehicle or CNO into LEC prior to the second test
416 phase, 48 h after labelling neurons.

417 Mice assigned to both vehicle and CNO groups showed intact memory at the 5 min delay (Fig.
418 2C, vehicle $t_{(9)} = 4.53$, $p = 0.001$; CNO $t_{(9)} = 5.73$, $p = 0.0003$). Critically, however, mice infused

419 with CNO prior to testing at 48 h had impaired memory, while vehicle infused mice had intact
420 memory (Fig. 2C, Drug by test phase $F_{(1,18)} = 21.92$, $p = 0.0002$; vehicle: $t_{(9)} = 10.39$, $p = 3.0 \times 10^{-6}$;
421 CNO: $t_{(9)} = -1.24$, $p = 0.12$). No difference in exploration levels were found between vehicle and
422 CNO groups at the sample (Fig. 2D, $F_{(1,18)} = 0.21$ $p = 0.656$) or either test phase (Fig. 2E, drug by
423 test phase $F_{(1,18)} = 4.50$, $p = 0.048$; vehicle vs CNO, test 1: $p = 0.194$, test 2: $p = 0.862$; T1 vs T2,
424 vehicle: $p = 2\times10^{-6}$, CNO: $p = 0.001$). These data demonstrate the necessity of LEC TRAP neurons
425 for successful retrieval of OiP memory, therefore definitively demonstrating their identity as
426 engram neurons.

427 **Object reconfiguration increases excitability of L5 LEC TRAP2 neurons**

428 Material changes in engram neurons are hypothesised to increase the likelihood of their
429 reactivation upon exposure to specific cues. One mechanism by which this can be achieved is
430 by changes in cellular excitability, which may facilitate firing in response to complete, partial or
431 ambiguous cues (Cai et al., 2016; Whitaker et al., 2017a; Pignatelli et al., 2019) and support
432 consolidation (Thompson et al., 1996; Zhang and Linden, 2003).

433 We investigated neuronal excitability in *TRAP2-Ai14* mice 48 h after TRAP labelling by preparing
434 *ex vivo* slices immediately after memory recall (Fig. 3A), focussing on deep-layer LEC neurons,
435 which had shown the highest levels of reactivation by OiP memory recall (Fig. 1G). In slices from
436 these mice, tdTom L5 pyramidal neurons exhibited increased firing in response to depolarising
437 current compared to unlabelled neurons (Fig. 3B). Further analysis of the physiological
438 properties of these neuronal populations (Fig. 3B; Table 2) showed input resistance was
439 significantly higher in tdTom neurons. Rheobase, a measure related to input resistance and
440 action potential threshold, was lower in tdTom neurons but not statistically different, likely
441 owing to an insignificant trend to a more depolarised action potential threshold in tdTom
442 neurons. Other membrane properties that influence firing, including afterhyperpolarisation
443 (AHP) potentials (Disterhoft and Oh, 2006; Whitaker et al., 2017b), were not significantly

444 different (Fig. 3B; Table 2). In addition to increased excitability, tdTom neurons also showed
445 modified action potential dynamics, exhibiting lower amplitude action potentials which had a
446 slower rate of rise than those observed in unlabelled neurons (Fig. 3B; Table 2). Collectively
447 these data show that exposure to a novel configuration of engram-related objects elicits
448 changes in the electrophysiological properties of tdTom neurons, resulting in increased
449 excitability and firing rate in response to depolarising stimuli.

450 **Excitability changes were not observed in other cortical engram cells**

451 That tdTom L5 LEC pyramidal neurons are both reactivated and show heightened excitability
452 following exposure to rearranged objects suggests a key role in OiP memory. We next asked
453 whether other neuronal populations activated by OiP memory also undergo changes in cellular
454 excitability. tdTom labelling was found to be abundant in LEC L2a fan cells, which are required
455 for episodic-like (Vandrey et al., 2020) and associative memory (Lee et al., 2021), in *ex vivo*
456 slices from mice exposed to reconfigured objects. However, unlike L5 pyramidal neurons, no
457 differences in spiking or other measures of intrinsic excitability or action potential waveforms
458 were found between tdTom and unlabelled L2a fan cells (Fig. 3C, Table 2).

459 We next examined excitability of pyramidal neurons in PRH, a major input to LEC which encodes
460 object identity and novelty (Seoane et al., 2012) but which, in contrast to LEC, is not thought to
461 encode object-location associations (Deshmukh et al., 2012). Labelling in PRH had a similar
462 pattern to that seen in in LEC: both Fos labelling (Fig. S1C) and tdTom cell reactivation (Fig. 1E)
463 after retrieval were elevated in OiP mice compared to FA, although reactivation of PRH engram
464 cells was not significantly correlated with memory performance (Fig. S1F). tdTom and Fos
465 labelling was higher in PRH L5/6 than L2/3 (Fig. S2F) irrespective of task, and reactivation was
466 enhanced in L5/6 compared to L2/3 in OiP mice only. However, no differences in action
467 potential firing or other electrophysiological parameters between tdTom and unlabelled PRH
468 neurons were observed (Fig. 3D, Table 3).

469 We additionally assessed excitability in mPFC, however no changes in the firing rate nor other
470 electrophysiological measures were found in L5 pyramidal cells (Fig. 3E, Table 4) or L2/3
471 pyramidal cells (Fig. 3F, Table 4). Together these data show that whilst OiP recall results in
472 significant reactivation of tdTom labelled neurons in multiple cortical regions and layers,
473 increases in cellular excitability and action potential dynamics were only found in L5 LEC
474 neurons.

475 **Increased neuronal excitability of TRAP2 LEC L5 pyramidal neurons requires recall of**
476 **engram-specific cues with associated novel information**

477 We next examined the behavioural conditions required to elicit changes in engram cell
478 excitability. Increased cellular excitability has been suggested as a mechanism either leading to,
479 or resulting from, recruitment to an engram (Disterhoft and Oh, 2006; Josselyn and Frankland,
480 2018); if such changes persist to 48 h after encoding, then these may explain the increased
481 excitability of LEC L5 tdTom neurons. We investigated this possibility by recording from LEC L5
482 pyramidal neurons 48 h after encoding, without recall prior to slicing (Fig. 4A). We found that
483 tdTom and unlabelled cells had equal rates of firing, cellular excitability and action potential
484 properties (Fig. 4A, Table 5). These data show that increased excitability of tdTom LEC L5
485 pyramidal cells requires re-exposure to the engram objects.

486 OiP recall in our experiments contains both static and displaced objects, thus the increased
487 excitability of LEC neurons may result from either memory recall or encoding of new
488 information. To determine whether excitability changes could be induced only by recall, mice
489 were re-exposed to the familiar object configuration (previously encountered in test phase 1)
490 immediately prior to slicing (Fig. 4B). Re-exposure to this familiar object configuration did not,
491 however, lead to any changes in firing or intrinsic electrophysiological properties (Fig. 4B, Table
492 6), suggesting that retrieval of specific cues in a familiar configuration does not alter engram cell
493 excitability.

These data suggest that changes in intrinsic excitability may be a mechanism by which novel information regarding object locations is integrated into the pre-existing engram as part of a reconsolidation-like process. Alternatively, the increased excitability in tdTom neurons may have been a response to a more general novelty signal created by object reconfiguration. To determine this, we presented mice with a previously unencountered set of objects at test phase 2 (Fig. 4C). No difference in firing rate or other measures of cellular excitability were observed in *ex vivo* slices from mice exposed to novel objects, however action potential dynamics showed similar changes (slower rate of rise, smaller amplitude) to those observed in slices from mice which had encountered rearranged engram-related objects (Fig. 4C, Table 7). These data demonstrate that whilst a novel object set can alter action potential dynamics, the increased cellular excitability and firing rates observed in response to object reconfiguration are engram-specific and are not a result of a general novelty signal.

Discussion

In this study we investigate the identity of cortical neurons encoding associative recognition memories, showing that engram cell recruitment and reactivation upon memory retrieval occurs across the lateral entorhinal, medial prefrontal and perirhinal cortices. However, within these regions, only the dorsal extent of the LEC showed a strong correlation between engram-cell reactivation and memory performance, and reactivation was higher in L5/6 DLent neurons. Furthermore, reactivation of LEC engram neurons was shown to be necessary for memory recall, and layer 5 LEC neurons exhibited enhanced intrinsic excitability following a memory-recall task. Crucially, increased excitability was contingent upon the object set having been

518 rearranged at recall whereas unmoved objects or a second set of objects did not increase
519 excitability. These data collectively implicate deep layer DLent neurons as crucial for object-
520 place associations, and increased excitability of these neurons may represent a novel
521 mechanism by which new information is integrated into an existing memory engram.

522 Recent studies using molecular-genetic activity-labelling have provided considerable support to
523 the notion of memory engrams as cellular substrates of memory (Josselyn and Tonegawa, 2020;
524 Ortega-de San Luis et al., 2023), however these investigations have relied on strongly aversive or
525 rewarding behaviours. Here we provide a detailed characterisation of cortical engrams for
526 associative recognition memory, a spontaneous, unrewarded, single-trial form of learning which
527 is critical to our everyday lives.

528 Our analysis showed that OiP produces robust activity-dependent labelling of neurons in
529 multiple recognition memory associated cortices. However, memory performance correlated
530 with reactivation of tdTom cells only in LEC, and this correlation exhibited a dorsal-ventral
531 gradient, with a strong correlation in DLent and no correlation in VIent. These data support the
532 notion that DLent can support object-place associations, in contrast with PRH, which is thought
533 to only encode object identity and novelty (Deshmukh et al., 2012) and in which no correlation
534 was found between reactivation and memory.

535 Within LEC, L5/6 neurons showed higher levels of reactivation than L2/3 neurons, despite
536 similar numbers of neurons in these regions being activated overall at encoding and recall; this
537 heightened level of reactivation combined with the intrinsic excitability plasticity seen in these
538 neurons implicates DLent L5/6 as a key locus of object-place associations. Whilst previous
539 studies have shown object-place representations in LEC L5/6 (Keene et al., 2016), most
540 evidence to date has implicated superficial LEC neurons in encoding associative (Lee et al.,
541 2021) and episodic-like memory (Vandrey et al., 2020). L5 LEC neurons are anatomically well
542 positioned within associative recognition memory circuitry, being the recipients of convergent

543 top-down feedback inputs from both dorsal hippocampus(Ohara et al., 2023) and inputs from
544 mPFC (Kinnavane and Banks, 2022; Kinnavane et al., 2025). Outputs from L5 LEC neurons
545 project to other telencephalic regions (Ohara et al., 2023), including mPFC (Hoover and Vertes,
546 2007), and locally within LEC where they target superficial layers (Ohara et al., 2021) which
547 project to hippocampus. Dorsal LEC L5 is, therefore, a key node in bidirectional loops between
548 LEC-hippocampus and LEC-mPFC.

549 The notion that deep-layer LEC neurons support object-place associations is supported by
550 plasticity of excitability which occurred specifically in LEC L5 TRAP2 pyramidal neurons
551 following exploration of reconfigured objects, which was absent in L2a fan cells, PRH L5, and
552 both L2/3 and L5 mPFC pyramidal neurons. This finding raises the possibility that plasticity of
553 cellular excitability in these neurons may represent a mechanism by which neural object-place
554 representations can be rapidly altered in response to engram-related environmental novelty.
555 Whilst changes in cellular excitability were only found in LEC L5, this is not to say that other
556 plastic changes, such as synaptic plasticity, do not occur in other cell populations (Ryan et al.,
557 2015; Lee et al., 2023; Tozzi et al., 2024).

558 Two alterations to LEC L5 tdTom$^+$ cells were found in this study: firstly, increased input
559 resistance, with an accompanying increase in firing upon depolarisation. A decrease in
560 potassium conductance is a potential mechanism for this increased excitability associated with
561 recall (Pignatelli et al., 2019), whereas other mechanisms regulating firing rate such as AHP
562 (Disterhoft and Oh, 2006; Cai et al., 2016) were unaltered. Secondly, we observed action
563 potentials had reduced amplitude and rate of rise, likely reflecting decreased voltage-gated
564 sodium channel function which has previously been observed in response to dopaminergic
565 activity (Cantrell and Catterall, 2001), which signals novelty in LEC (Lee et al., 2021).

566 Increased engram cell excitability was only observed under specific conditions. The absence of
567 plasticity in tdTom$^+$ cells from mice which did not re-encounter objects before slicing shows

568 that increased excitability either leading to, or resulting from, recruitment to an engram
569 (Disterhoft and Oh, 2006; Josselyn and Frankland, 2018) either did not occur or was not
570 persistent 48 h later. Furthermore, as we found no electrophysiological difference between
571 engram and non-engram cells when no recall had taken place before slicing, it is unlikely that
572 engram recruitment is biased towards a particular subclass of LEC L5 pyramidal cells, which
573 have different electrophysiological phenotypes, such as layer 5a vs 5b pyramidal cells (Ohara et
574 al., 2021).

575 Re-exposure to objects in familiar locations did not alter engram cell excitability. Meanwhile,
576 exploration of completely novel objects resulted only in altered action potential dynamics. We
577 hypothesize that a novelty signal, such as release of neuromodulatory transmitter, may be
578 sufficient to induce changes in action potential dynamics in both the novel objects and
579 reconfigured objects groups, but that this novelty signal must be accompanied by strong
580 activation of synapses within the engram network, including from engram cells in neurons from
581 distal regions such as mPFC and hippocampus, to generate a plasticity signal that results in
582 increased firing.

583 The function of intrinsic plasticity in engram cells is unclear. Evidence suggests that engram cell
584 intrinsic excitability increases during a short temporal window after memory recall, and that
585 these changes facilitate pattern separation and completion (Pignatelli et al., 2019). Heightened
586 excitability may therefore act as a (likely temporary) mechanism of updating environmental
587 representations by integrating new information into an established engram via a re-
588 consolidation like process, and may facilitate processes underlying systems consolidation
589 (such as replay events (Olafsdottir et al., 2018)) which facilitate longer term storage of
590 environmental changes in the form of synaptic changes (Ryan et al., 2015; Lee et al., 2023).

591

592

Additional resources

Data and code used in this manuscript are available upon request.

Author Contributions

Research was designed by: P.J.B., G.R.I.B., E.C.W. and Z.I.B. Research was performed by: P.J.B., G.R.I.B., C.A.B. and L.K. Data analysis was performed by: P.J.B., G.R.I.B. and C.A.B. The first draft of the paper was written by P.J.B., review and editing of the paper was performed by: P.J.B., G.R.I.B., C.A.B., E.C.W. and Z.I.B.

References

Aggleton JP, Nelson AJD (2020) Distributed interactive brain circuits for object-in-place memory: A place for time? Brain Neurosci Adv 4:2398212820933471.

Allen WE, DeNardo LA, Chen MZ, Liu CD, Loh KM, Fenno LE, Ramakrishnan C, Deisseroth K, Luo L (2017) Thirst-associated preoptic neurons encode an aversive motivational drive. Science 357:1149-1155.

Anastasiades PG, Boada C, Carter AG (2019) Cell-Type-Specific D1 Dopamine Receptor Modulation of Projection Neurons and Interneurons in the Prefrontal Cortex. Cereb Cortex 29:3224-3242.

Anderson WW, Collingridge GL (2007) Capabilities of the WinLTP data acquisition program extending beyond basic LTP experimental functions. J Neurosci Methods 162:346-356.

Barbosa FF, Santos JR, Meurer YS, Macedo PT, Ferreira LM, Pontes IM, Ribeiro AM, Silva RH (2013) Differential Cortical c-Fos and Zif-268 Expression after Object and Spatial Memory Processing in a Standard or Episodic-Like Object Recognition Task. Front Behav Neurosci 7:112.

615 Barker GR, Bashir ZI, Brown MW, Warburton EC (2006) A temporally distinct role for group I and
616 group II metabotropic glutamate receptors in object recognition memory. Learn Mem
617 13:178-186.
618 Barker GR, Banks PJ, Scott H, Ralph GS, Mitrophanous KA, Wong LF, Bashir ZI, Uney JB,
619 Warburton EC (2017) Separate elements of episodic memory subserved by distinct
620 hippocampal-prefrontal connections. Nat Neurosci 20:242-250.
621 Barker GRI, Bird F, Alexander V, Warburton EC (2007) Recognition Memory for Objects, Place,
622 and Temporal Order: A Disconnection Analysis of the Role of the Medial Prefrontal
623 Cortex and Perirhinal Cortex. J Neurosci 27:2948-2957.
624 Bobadilla AC, Dereschewitz E, Vaccaro L, Heinsbroek JA, Scofield MD, Kalivas PW (2020)
625 Cocaine and sucrose rewards recruit different seeking ensembles in the nucleus
626 accumbens core. Mol Psychiatry 25:3150-3163.
627 Cai DJ et al. (2016) A shared neural ensemble links distinct contextual memories encoded close
628 in time. Nature 534:115-118.
629 Cantrell AR, Catterall WA (2001) Neuromodulation of Na+ channels: an unexpected form of
630 cellular plasticity. Nat Rev Neurosci 2:397-407.
631 Chao OY, Huston JP, Li JS, Wang AL, de Souza Silva MA (2016) The medial prefrontal cortex-
632 lateral entorhinal cortex circuit is essential for episodic-like memory and associative
633 object-recognition. Hippocampus 26:633-645.
634 Davies JJ, M.G.; Hinchcliffe, J.K.; Mendl, M.; Robinson, E.S.J. (2025) Male mice prefer to live on
635 their own. BioRxiv:21.
636 Davies JR, Purawijaya DA, Bartlett JM, Robinson ESJ (2022) Impact of Refinements to Handling
637 and Restraint Methods in Mice. Animals (Basel) 12.
638 DeNardo LA, Liu CD, Allen WE, Adams EL, Friedmann D, Fu L, Guenthner CJ, Tessier-Lavigne M,
639 Luo L (2019) Temporal evolution of cortical ensembles promoting remote memory
640 retrieval. Nat Neurosci 22:460-469.

641 Deshmukh SS, Knierim JJ (2011) Representation of non-spatial and spatial information in the
642 lateral entorhinal cortex. Front Behav Neurosci 5:69.
643 Deshmukh SS, Johnson JL, Knierim JJ (2012) Perirhinal cortex represents nonspatial, but not
644 spatial, information in rats foraging in the presence of objects: comparison with lateral
645 entorhinal cortex. Hippocampus 22:2045-2058.
646 Disterhoft JF, Oh MM (2006) Learning, aging and intrinsic neuronal plasticity. Trends Neurosci
647 29:587-599.
648 Dix S, Aggleton J (1999) Extending the spontaneous preference test of recognition: evidence of
649 object-location and object-context recognition. Behav Brain Res 99:191-200.
650 Eichenbaum H, Yonelinas AP, Ranganath C (2007) The Medial Temporal Lobe and Recognition
651 Memory. Annual Review of Neuroscience 30:123-152.
652 Ennaceur A, Delacour J (1988) A new one-trial test for neurobiological studies of memory in rats.
653 1: Behavioral data. Behav Brain Res 31:47-59.
654 Ennaceur A, Neave N, Aggleton J (1997) Spontaneous object recognition and object location
655 memory in rats: the effects of lesions in the cingulate cortices, the medial prefrontal
656 cortex, the cingulum bundle and the fornix. Exp Brain Res 113:509-519.
657 Hoover WB, Vertes RP (2007) Anatomical analysis of afferent projections to the medial
658 prefrontal cortex in the rat. Brain Struct Funct 212:149-179.
659 Josselyn SA, Frankland PW (2018) Memory Allocation: Mechanisms and Function. Annu Rev
660 Neurosci 41:389-413.
661 Josselyn SA, Tonegawa S (2020) Memory engrams: Recalling the past and imagining the future.
662 Science 367.
663 Keene CS, Bladon J, McKenzie S, Liu CD, O'Keefe J, Eichenbaum H (2016) Complementary
664 Functional Organization of Neuronal Activity Patterns in the Perirhinal, Lateral
665 Entorhinal, and Medial Entorhinal Cortices. J Neurosci 36:3660-3675.

666 Kerrigan TL, Brown JT, Randall AD (2014) Characterization of altered intrinsic excitability in
667 hippocampal CA1 pyramidal cells of the Abeta-overproducing PDAPP mouse.
668 Neuropharmacology 79:515-524.
669 Kinnavane L, Banks PJ (2022) Ex Vivo Optogenetic Interrogation of Long-Range Synaptic
670 Transmission and Plasticity from Medial Prefrontal Cortex to Lateral Entorhinal Cortex. J
671 Vis Exp.
672 Kinnavane L, Barker GRI, Banks PJ, Bashir ZI, Warburton EC (2025) Medial prefrontal cortex input
673 to lateral entorhinal cortex supports both encoding and retrieval of associative
674 recognition memory. BioRxiv.
675 Lee JH, Kim WB, Park EH, Cho JH (2023) Neocortical synaptic engrams for remote contextual
676 memories. Nat Neurosci 26:259-273.
677 Lee JY, Jun H, Soma S, Nakazono T, Shiraiwa K, Dasgupta A, Nakagawa T, Xie JL, Chavez J, Romo
678 R, Yungblut S, Hagihara M, Murata K, Igarashi KM (2021) Dopamine facilitates
679 associative memory encoding in the entorhinal cortex. Nature 598:321-326.
680 Madisen L, Zwingman TA, Sunkin SM, Oh SW, Zariwala HA, Gu H, Ng LL, Palmiter RD, Hawrylycz
681 MJ, Jones AR, Lein ES, Zeng H (2010) A robust and high-throughput Cre reporting and
682 characterization system for the whole mouse brain. Nat Neurosci 13:133-140.
683 Nilssen ES, Doan TP, Nigro MJ, Ohara S, Witter MP (2019) Neurons and networks in the
684 entorhinal cortex: A reappraisal of the lateral and medial entorhinal subdivisions
685 mediating parallel cortical pathways. Hippocampus 29:1238-1254.
686 Ohara S, Rannap M, Tsutsui KI, Draguhn A, Egorov AV, Witter MP (2023) Hippocampal-medial
687 entorhinal circuit is differently organized along the dorsoventral axis in rodents. Cell Rep
688 42:112001.
689 Ohara S, Blankvoort S, Nair RR, Nigro MJ, Nilssen ES, Kentros C, Witter MP (2021) Local
690 projections of layer Vb-to-Va are more prominent in lateral than in medial entorhinal
691 cortex. Elife 10.

Olafsdottir HF, Bush D, Barry C (2018) The Role of Hippocampal Replay in Memory and Planning. Curr Biol 28:R37-R50.

Ortega-de San Luis C, Pezzoli M, Urrieta E, Ryan TJ (2023) Engram cell connectivity as a mechanism for information encoding and memory function. Curr Biol 33:5368-5380 e5365.

Paxinos G, Franklin KBJ (2019) Paxinos and Franklin's the Mouse Brain in Stereotaxic Coordinates, Compact, 5th Edition: Academic Press.

Pignatelli M, Ryan TJ, Roy DS, Lovett C, Smith LM, Muralidhar S, Tonegawa S (2019) Engram Cell Excitability State Determines the Efficacy of Memory Retrieval. Neuron 101:274-284 e275.

Preston AR, Eichenbaum H (2013) Interplay of hippocampus and prefrontal cortex in memory. Curr Biol 23:R764-773.

Ryan TJ, Roy DS, Pignatelli M, Arons A, Tonegawa S (2015) Memory. Engram cells retain memory under retrograde amnesia. Science 348:1007-1013.

Seoane A, Tinsley CJ, Brown MW (2012) Interfering with Fos expression in rat perirhinal cortex impairs recognition memory. Hippocampus.

Stachniak TJ, Ghosh A, Sternson SM (2014) Chemogenetic synaptic silencing of neural circuits localizes a hypothalamus-->midbrain pathway for feeding behavior. Neuron 82:797-808.

Tahvildari B, Alonso A (2005) Morphological and electrophysiological properties of lateral entorhinal cortex layers II and III principal neurons. J Comp Neurol 491:123-140.

Tanaka KZ, Pevzner A, Hamidi AB, Nakazawa Y, Graham J, Wiltgen BJ (2014) Cortical representations are reinstated by the hippocampus during memory retrieval. Neuron 84:347-354.

Thompson LT, Moyer JR, Jr., Disterhoft JF (1996) Transient changes in excitability of rabbit CA3 neurons with a time course appropriate to support memory consolidation. J Neurophysiol 76:1836-1849.

Tozzi F, Guglielmo S, Paraciani C, van den Oever MC, Mainardi M, Cattaneo A, Origlia N (2024) Involvement of a lateral entorhinal cortex engram in episodic-like memory recall. Cell Rep 43:114795.

Tsao A, Sugar J, Lu L, Wang C, Knierim JJ, Moser MB, Moser EI (2018) Integrating time from experience in the lateral entorhinal cortex. Nature 561:57-62.

Van Cauter T, Camon J, Alvernhe A, Elduayen C, Sargolini F, Save E (2013) Distinct roles of medial and lateral entorhinal cortex in spatial cognition. Cereb Cortex 23:451-459.

Vandrey B, Garden DLF, Ambrozova V, McClure C, Nolan MF, Ainge JA (2020) Fan Cells in Layer 2 of the Lateral Entorhinal Cortex Are Critical for Episodic-like Memory. Curr Biol 30:169-175 e165.

Wang C, Chen X, Knierim JJ (2020) Egocentric and allocentric representations of space in the rodent brain. Curr Opin Neurobiol 60:12-20.

Wang C, Lee H, Rao G, Knierim JJ (2024) Multiplexing of temporal and spatial information in the lateral entorhinal cortex. Nat Commun 15:10533.

Wang C, Chen X, Lee H, Deshmukh SS, Yoganarasimha D, Savelli F, Knierim JJ (2018) Egocentric coding of external items in the lateral entorhinal cortex. Science 362:945-949.

Whitaker LR, Warren BL, Venniro M, Harte TC, McPherson KB, Beidel J, Bossert JM, Shaham Y, Bonci A, Hope BT (2017a) Bidirectional Modulation of Intrinsic Excitability in Rat Prelimbic Cortex Neuronal Ensembles and Non-Ensembles after Operant Learning. J Neurosci 37:8845-8856.

Whitaker LR, Warren BL, Venniro M, Harte TC, McPherson KB, Beidel J, Bossert JM, Shaham Y, Bonci A, Hope BT (2017b) Bidirectional Modulation of Intrinsic Excitability in Rat Prelimbic Cortex Neuronal Ensembles and Non-Ensembles after Operant Learning. Journal of Neuroscience 37:8845-8856.

Wilson DI, Watanabe S, Milner H, Ainge JA (2013) Lateral entorhinal cortex is necessary for associative but not nonassociative recognition memory. Hippocampus 23:1280-1290.

Zhang W, Linden DJ (2003) The other side of the engram: experience-driven changes in neuronal intrinsic excitability. Nat Rev Neurosci 4:885-900.

Zhu H, Aryal DK, Olsen RH, Urban DJ, Swearingen A, Forbes S, Roth BL, Hochgeschwender U (2016) Cre-dependent DREADD (Designer Receptors Exclusively Activated by Designer Drugs) mice. Genesis 54:439-446.

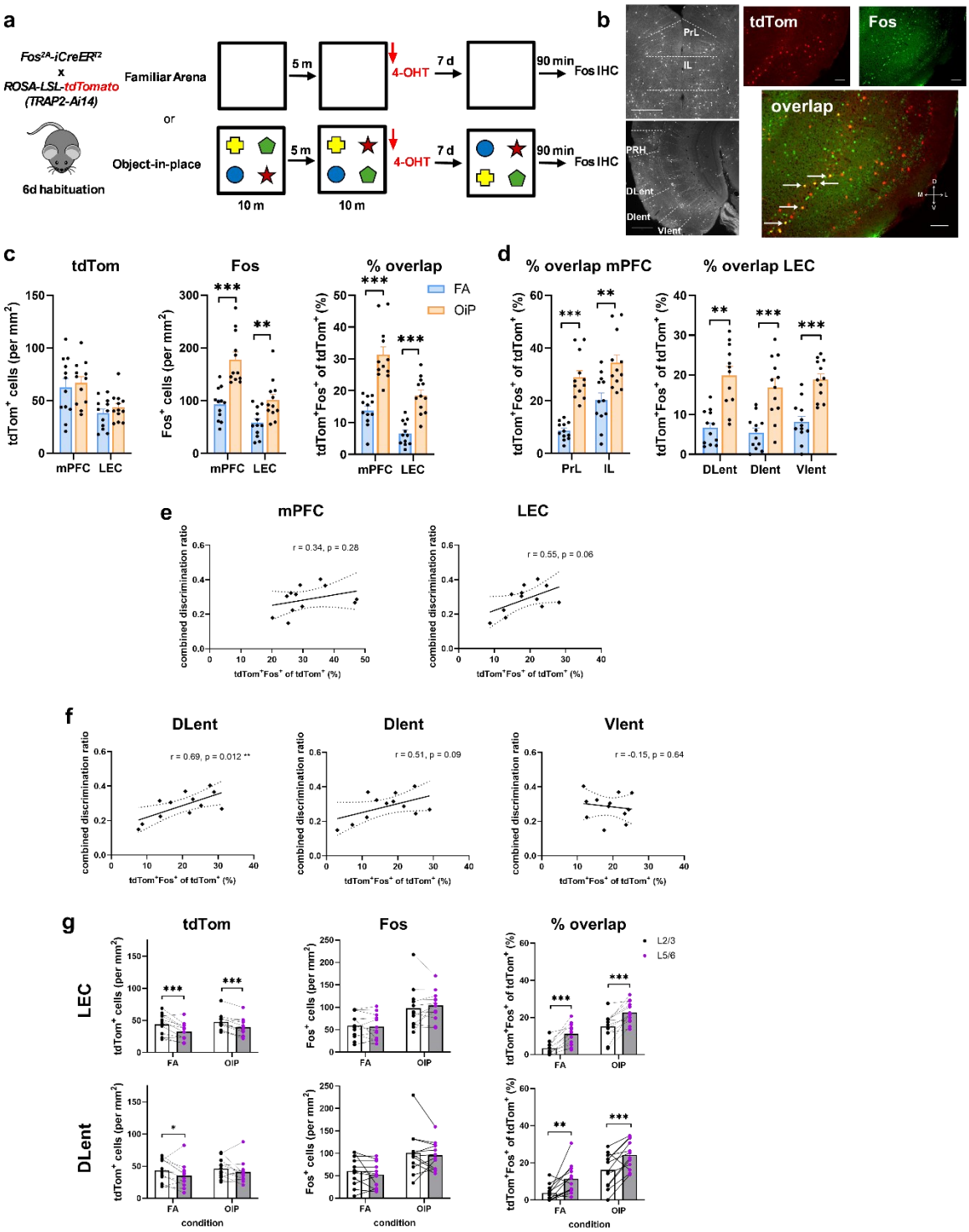

Figure 1: Reactivation of a dorsal lateral entorhinal cortex engram correlates with associative recognition memory performance. a: Experimental outline for associative memory-induced engram cell labelling. **b**: (Left) example OiP induced tdTom labelling in mPFC (upper) and LEC (lower) scale bar: 500 µm. (Right) example tdTom, Fos and overlap in LEC, arrows indicate cells expressing both tdTom and Fos; scale bar: 100 µm. **c**: (Left to right) tdTom

expression, Fos expression and percent overlap in mPFC and LEC for FA and OiP behavioural conditions. **d**: Percent overlap of tdTom and Fos in mPFC subregions PrL and IL and LEC subregions DLent, DIent and VIent. **e**: Correlation between tdTom/Fos overlap and memory performance (combined discrimination ratio) in OiP behavioural task for mPFC and LEC. Dashed line show 95% confidence intervals. **f**: Same as (E) for LEC subregions. **g**: Expression levels of tdTom (left), Fos (middle) and overlap (right) in L2/3 and L5/6 of LEC (top) and DLent (bottom). Bar charts indicate mean + SEM* $p < 0.05$, ** $p < 0.01$, *** $p < 0.001$. N = 12 mice for all experiments.. See Supplementary Data Tables 1 & 2 for detailed statistical analysis.

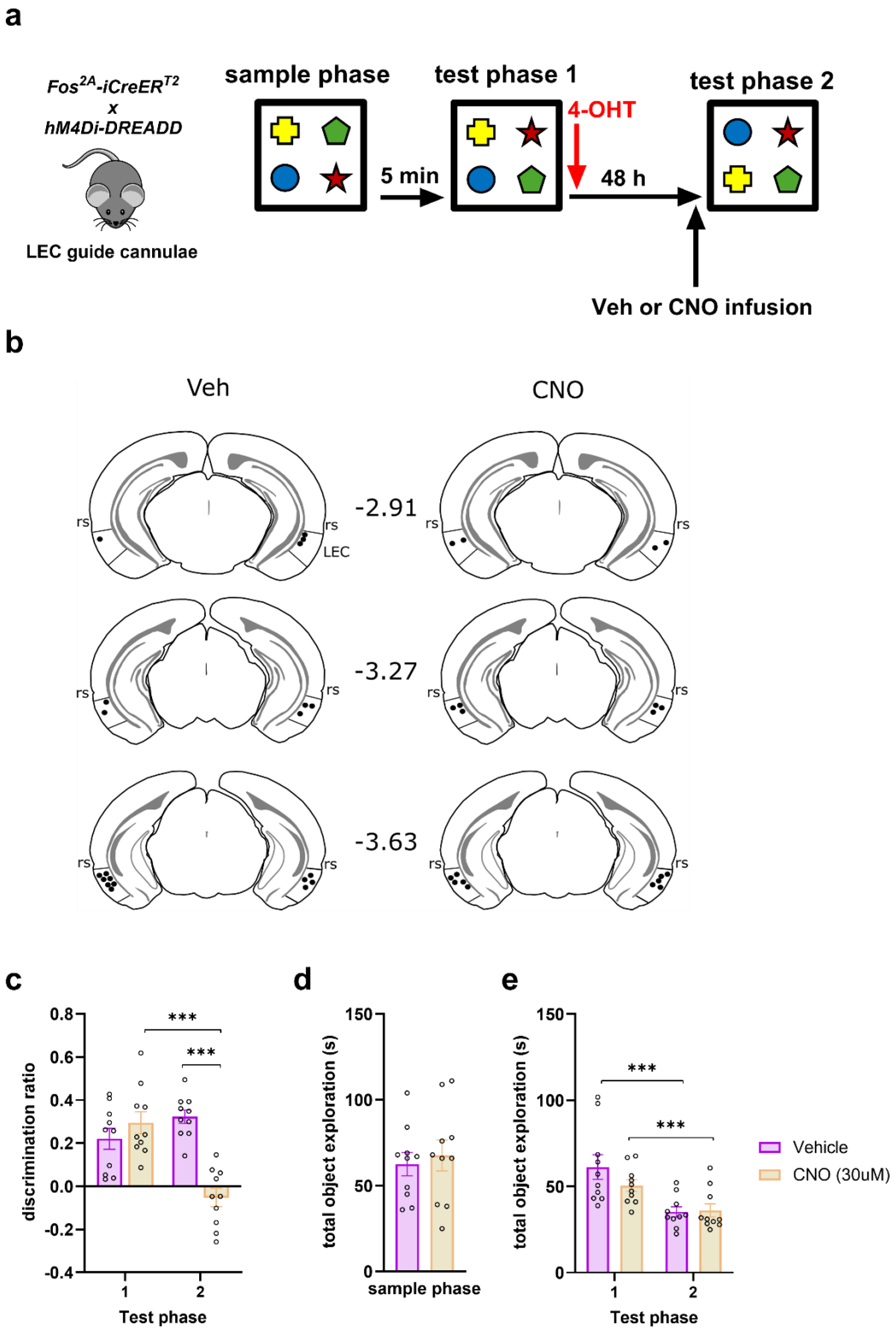

769

770 **Figure 2: Engram cells in lateral entorhinal cortex are essential for the retrieval of**

771 **associative recognition memory. a**: Experimental outline for deactivating LEC engram cells

772 during associative recognition memory retrieval. **b**: LEC cannula locations (represented by black

773 dots) in the vehicle (left) and CNO (right) infused animals. Numbers represent AP position in mm
774 relative to bregma. rs = rhinal sulcus. **c**: Memory performance (discrimination ratio) at test phase
775 1 and test phase 2 of vehicle and CNO infused animals. **d**: Total object exploration during the
776 sample phase of the OiP task. **e**: Total object exploration levels during test phase 1 and test phase
777 2 of the object in place task. Bar charts show mean ± SEM. *** $p<0.001$. N = 10 mice for all
778 conditions. For statistical analysis see text.

779

780

781

782

783

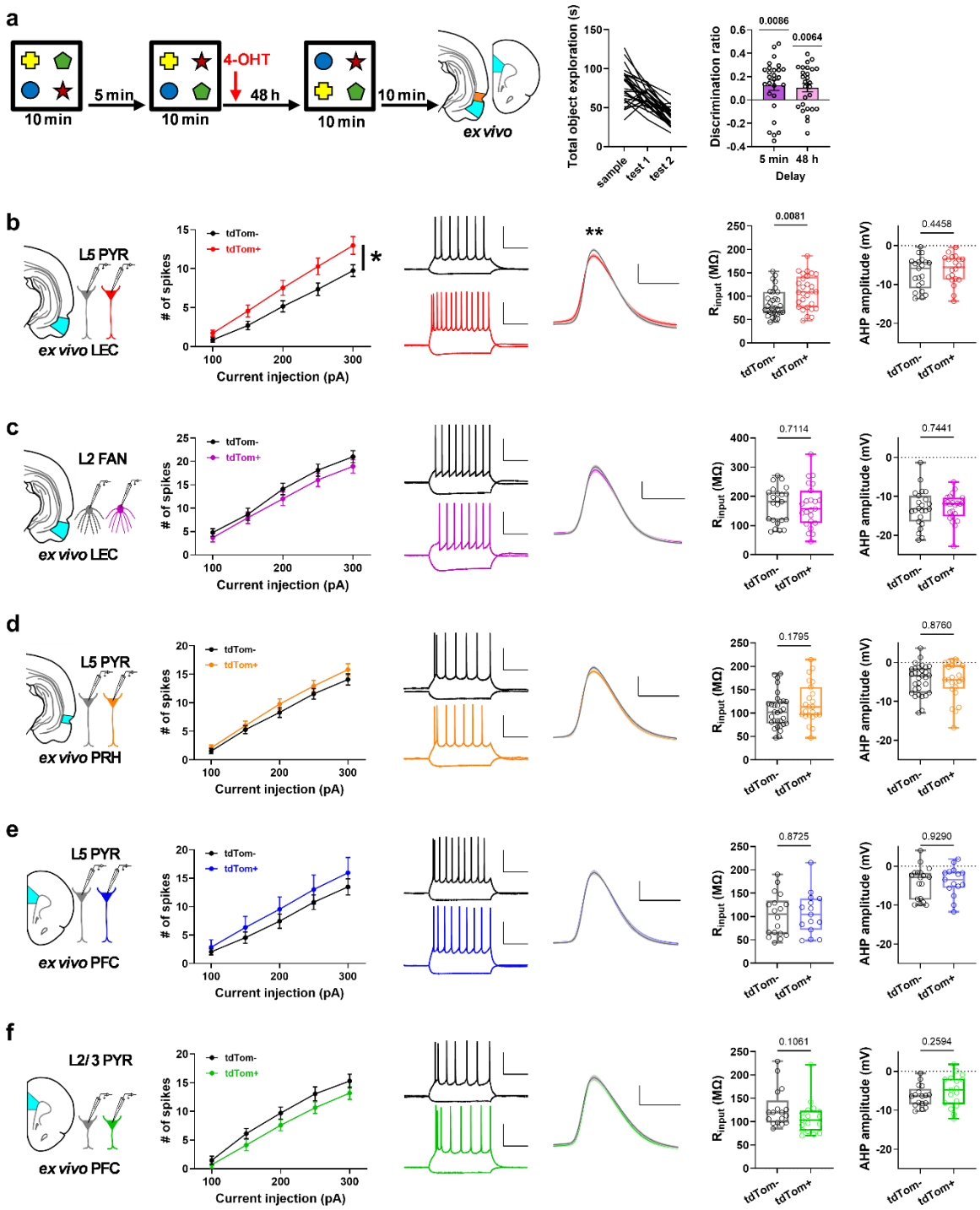

Figure 3. Object reconfiguration increases excitability of LEC L5 pyramidal engram cells, but not other cortical engram cells

a: (Left) Experimental schematic for *ex vivo* recordings from animals exposed to reconfigured objects before slicing. (Right) exploration and discrimination ratio, bars represent mean ± SEM (n = 27 mice). **b**: Left to right: action potential firing (mean ± SEM), representative voltage

responses to -100 and +200 pA current injections for a tdTom$^-$ and tdTom$^+$ cell pair, average action potential waveforms, input resistance and afterhyperpolarisation (AHP) amplitude of LEC L5 pyramidal neurons. Boxplots show median (centre line), 25th and 75th percentiles, whiskers show minimum and maximum points. tdTom$^-$ n = 31 cells from 16 mice, tdTom$^+$ n = 28 cells from 16 mice. **c**: Same as (**b**) but for L2 fan cells. tdTom$^-$ n = 23 cells from 16 mice, tdTom$^+$ n = 23 cells from 17 mice. **d**: Same as (**b**) but for perirhinal cortex L5 pyramidal cells. tdTom$^-$ n = 31 cells from 14 mice, tdTom$^+$ n = 23 cells from 13 mice. **e**: Same as (**b**) but for prefrontal cortex L5 pyramidal cells. tdTom$^-$ n = 18 cells from 5 mice, tdTom$^+$ n = 15 cells from 5 mice. **f**: Same as (**b**) but for prefrontal cortex L2/3 pyramidal cells. tdTom$^-$ n = 17 cells from 5 mice, tdTom$^+$ n = 17 cells from 5 mice. Scale bars 200 ms, 40 mV. * = $p<0.05$, ** = $p < 0.01$. See Supplementary Data Tables 3-5 for further parameters and statistical analysis.

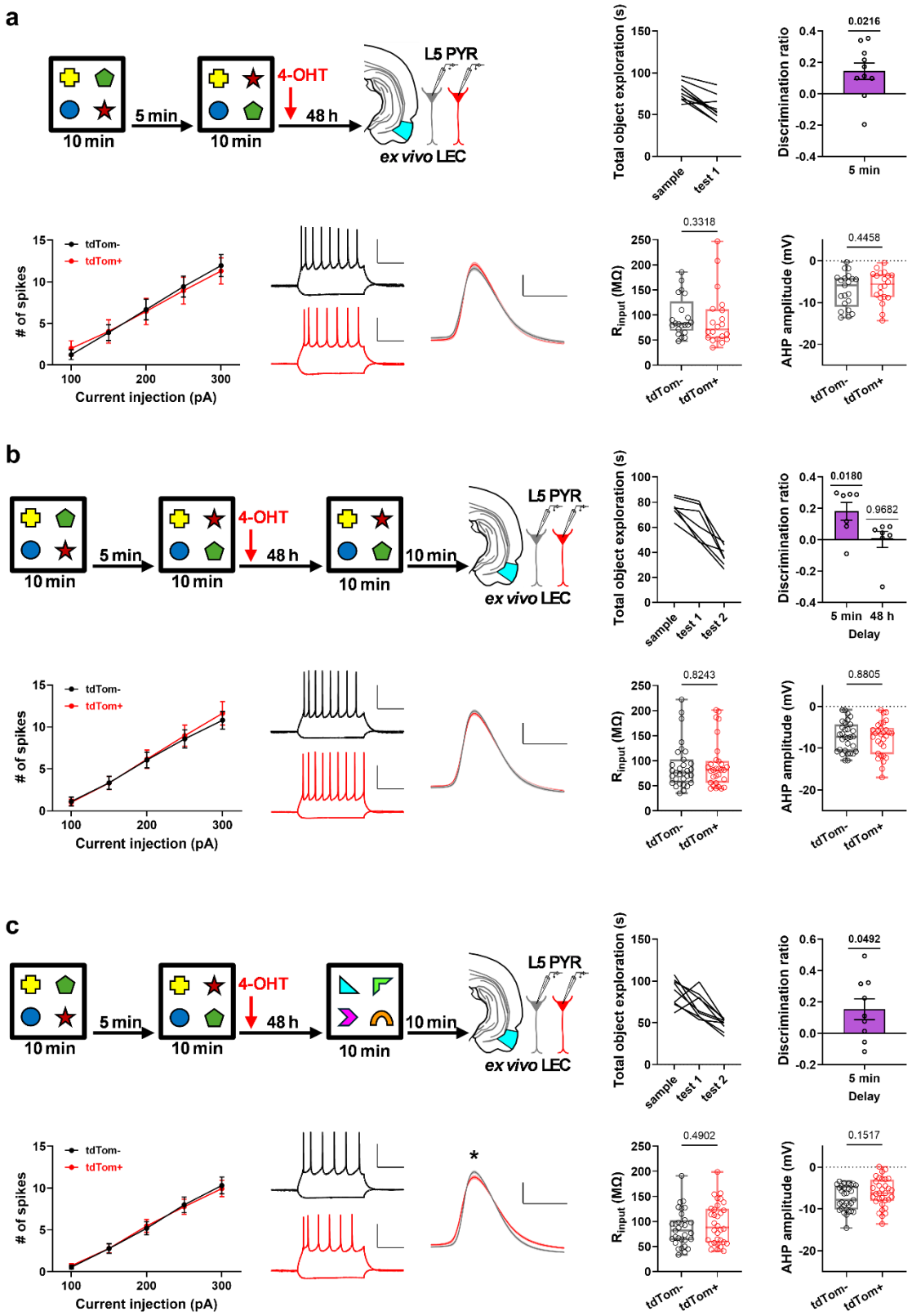

822

823 **Figure 4. Increased neuronal excitability of LEC L5 pyramidal neurons requires recall of**

824 **engram specific cues with associated novel information. a,** *Top*: Schematic and behavioural

825 data for *ex vivo* recordings from mice which were not presented with a second test phase before
826 slicing, bars represent mean ± SEM (n = 10 mice). *Bottom:* action potential firing (mean ± SEM),
827 representative voltage responses to -100 and +200 pA current injections for a $tdTom^-$ and $tdTom^+$
828 cell pair, average action potential waveforms, input resistance and afterhyperpolarisation (AHP)
829 amplitude of LEC L5 pyramidal neurons. Boxplots show median (centre line), 25th and 75th
830 percentiles, whiskers show minimum and maximum points. $tdTom^-$ n = 21 cells from 10 mice,
831 $tdTom^+$ n = 20 cells from 10 mice. **b.** Same as (a) but mice shown familiar object configuration
832 before slicing. $tdTom^-$ n = 31 cells from 7 mice, $tdTom^+$ n = 30 cells from 7 mice. **c**. Same as (a)
833 but mice shown a novel object set before slicing. $tdTom^-$ n = 31 cells from 9 mice, $tdTom^+$ n = 32
834 cells from 9 mice. Scale bars 200 ms, 40 mV. * = $p<0.05$. See Supplementary Data Tables 6-8 for
835 further parameters and statistical analysis.

836
837
838
839
840
841
842
843
844
845
846
847
848
849
850
851
852

Section	AP position, relative to bregma	Brain regions analysed
mPFC 1	+2.33mm to +1.97mm	PrL
mPFC 2	+1.97mm to +1.77mm	PrL, IL
mPFC 3	+1.77mm to +1.41mm	PrL, IL
mPFC 4	+1.41mm to +1.33mm	IL
LEC 1	-2.91mm to -3.15mm	PRH, DLent, DIent
LEC 2	-3.15mm to -3.27mm	PRH, DLent, DIent
LEC 3	-3.39mm to -3.63mm	PRH, DLent, DIent, VIent
LEC 4	-3.79mm to -4.10mm	PRH, DLent, DIent, VIent
LEC 5	-4.23mm to -4.47mm	PRH, DLent, DIent, VIent

Table 1: Anterior-posterior position relative to bregma of coronal sections analysed for tdTom and Fos expression and overlap. PrL prelimbic cortex, IL infralimbic cortex, PRH perirhinal cortex, DLent dorsal lateral entorhinal cortex, DIent dorsal intermediate entorhinal cortex, VIent ventral intermediate entorhinal cortex.

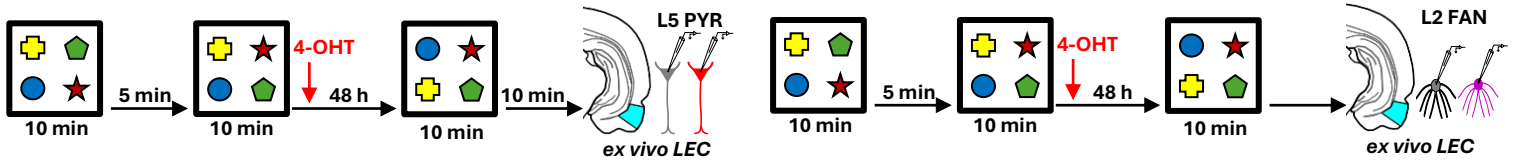

Physiological property	tdTom- L5 LEC pyramidal cells	tdTom+ L5 LEC pyramidal cells	Mann Whitney U	P-value	tdTom- L2 fan cells	tdTom+ L2 fan cells	Mann Whitney U	P-value
n (cells, mice)	31, 16	28, 16			23, 16	23,17		
n cells (DLE, DIE, VIE)	22, 9, 0	18, 9, 1			10, 11, 2	12, 10, 1		
RMP (mV)	-64.9 (-67.0,-62.0)	-64.2 (-66.4,-61.3)	379	0.409	-63.8 (-67.6,-62.1)	-63.4 (-66.2,-58.5)	205.5	0.199
R_{input} (MΩ)	74.9 (63.8,108.9)	108.7 (76.3,141.7)	261	0.0081	198.2 (129.0,247.6)	156.9 (108.7,219.2)	210	0.238
Tau (ms)	20.3 (14.3,25.5)	19.1 (15.6,22.4)	376	0.386	21.1 (16.7,25.0)	21.2 (15.0,27.3)	255	0.845
Sag (%)	13.3 (5.3,22.1)	14.6 (6.1,18.7)	418	0.815	15.3 (8.7,19.4)	13.4 (7.2,20.5)	241	0.617
Rheobase (pA)	167.3 (107.1,221.0)	135.3 (85.2,188.0)	347	0.191	75.9 (47.3,133.8)	95.7 (52.1,144.0)	235	0.528
AP threshold (mV)	-38.9 (-42.4,-34.9)	-37.0 (-39.2,-33.1)	318	0.0795	-40.8 (-46.1,-39.2)	-42.1 (-43.5,-39.4)	248	0.728
AHP (mV)	-7.8 (-9.7,-4.7)	-6.1 (-10.1,-2.6)	380	0.420	-13.2 (-16.5,-9.9)	-12.0 (-15.1,-10.4)	249	0.744
mAHP amplitude (mV)	-2.6 (-3.7,-1.0)	-1.8 (-2.9,-1.0)	374	0.369	-1.5 (-2.0,-0.7)	-1.3 (-1.7,-0.3)	212	0.256
mAHP area (mV.ms)	-0.20 (-0.28,-0.07)	-0.14 (-0.23,-0.07)	377	0.394	-0.13 (-0.15,-0.05)	-0.10 (-0.13,-0.02)	208	0.221
ADP presence (#cells)	14/31	11/28	χ^2 = 0.21	0.648	6/23	9/23	χ^2 = 0.89	0.345
ADP amplitude (mV)	0.18 (0.10,0.86)[a]	0.31 (0.17,1.46)	42	0.093	0.33 (0.07,0.66)	0.15 (0.07,0.45)	26	0.955
AP amplitude (mV)	74.8 (70.0,82.4)	66.1 (58.6,77.4)	247	0.0041	81.0 (69.0,84.6)	78.3 (58.5,85.0)	217	0.305
AP half width (ms)	0.81 (0.74,0.95)	0.84 (0.77,0.98)	361	0.273	0.80 (0.75,0.97)	0.82 (0.75,0.95)	250	0.761
AP max RoR ($mV.ms^{-1}$)	327 (263,414)	249 (208,350)	271	0.013	344 (266,375)	310 (210,379)	232.5	0.489
Cell firing	**Mixed-effects model**	**Factor**	**F**	**P-value**	**Mixed-effects model**	**Factor**	**F**	**P-value**
		Current	$F_{(1.4, 80)}$ = 268	$<1x10^{-15}$		Current	$F_{(2.0, 85.5)}$ = 384	$<1x10^{-15}$
		Labelling	$F_{(1, 57)}$ = 4.92	0.031		Labelling	$F_{(1,44)}$ = 1.00	0. 32
		Interaction	$F_{(4,228)}$ = 3.72	0.006		Interaction	$F_{(4,174)}$ = 0.77	0.55

Table 2. Summary of physiological properties of LEC layer 5 pyramidal and layer 2 fan tdTom- and tdTom+ neurons recorded from ex vivo slices from animals which underwent a second test phase (related to Fig. 3b,c). Values represent median (25,75 percentiles). Reported statistical values show Mann Whitney U test with 2-tailed p-value, except for ADP presence which uses Chi-squared test with 2-tailed p value. [a]*one cell was excluded from analysis due to spiking during ADP*. RMP resting membrane potential, R_{input} input resistance, AP action potential, AHP afterspike-hyperpolarisation, mAHP medium AHP, ADP afterspike-depolarisation, RoR rate of rise.

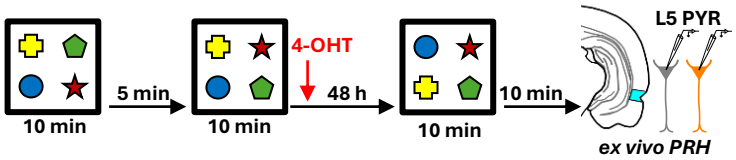

Physiological property	tdTom- L5 PRH pyramidal cells	tdTom+ L5 PRH pyramidal cells	Mann Whitney U	P-value
n (cells, mice)	31, 14	23, 13		
RMP (mV)	-63.8 (-66.3,-60.8)	-64.0 (-66.3,-61.2)	330.5	0.655
R_{input} (MΩ)	102.0 (78.0,124.6)	113.2 (95.7,155.4)	279	0.180
Tau (ms)	17.8 (15.0,22.1)	18.0 (14.1,23.4)	351	0.931
Sag (%)	15.4 (9.5,19.2)	14.0 (10.2,20.2)	355	0.986
Rheobase (pA)	117.4 (84.2,158.2)[a]	104.7 (86.0,166.8)[a]	290	0.785
AP threshold (mV)	-39.2 (-41.6,-37.3)	-39.8 (-41.5,-37.4)	310	0.424
AHP (mV)	-3.5 (-7.8,-1.5)	-4.4 (-6.8,-0.8)	347	0.876
mAHP amplitude (mV)	-2.6 (-3.6,-1.2)	-2.5 (-3.3,-1.3)	355	0.986
mAHP area (mV.ms)	-0.19 (-0.29,-0.07)	-0.17 (-0.27,-0.09)	352	0.945
ADP presence (#cells)	12/31	11/23	$\chi^2 = 0.45$	0.503
ADP amplitude (mV)	0.31 (0.09,0.71)	0.13 (0.05,0.89)	58	0.651
AP amplitude (mV)	71.5 (65.1,79.2)	66.8 (63.7,71.7)	251	0.066
AP half width (ms)	0.89 (0.81,1.05)	0.92 (0.83,1.02)	327	0.615
AP max RoR ($mV.ms^{-1}$)	273 (212,344)	256 (211,286)	270	0.133
		Factor	**F**	**P-value**
Cell firing	**Mixed-effects model**	Current	$F_{(1.5, 74.9)} = 415$	$<1x10^{-15}$
		Labelling	$F_{(1,52)} = 1.04$	0.31
		Interaction	$F_{(4,207)} = 0.87$	0.48

Table 3. Summary of physiological properties of layer 5 perirhinal cortex tdTom- and tdTom+ neurons recorded from ex vivo slices from animals which underwent a second test phase (related to Fig. 3d). Values represent median (25,75 percentiles). Reported statistical values show Mann Whitney U test with 2-tailed p-value, except for ADP presence which uses Chi-squared test with 2-tailed p value. [a]*data not collected for 2 cells*. RMP resting membrane potential, Rinput input resistance, AP action potential, AHP afterspike-hyperpolarisation, mAHP medium AHP, ADP afterspike-depolarisation, RoR rate of rise

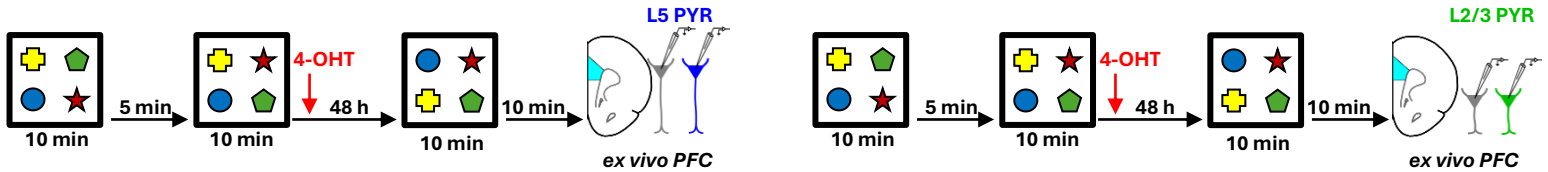

Physiological property	tdTom- L5 mPFC pyramidal cells	tdTom+ L5 mPFC pyramidal cells	Mann Whitney U	P-value	tdTom- L2/3 PFC pyramidal cells	tdTom+ L2/3 PFC pyramidal cells	Mann Whitney U	P-value
n (cells, mice)	18, 5	18, 5			17, 5	17, 5		
RMP (mV)	-64.2 (-66.2,-63.1)	-64.9 (-67.4,-61.8)	127	0.782	-64.3 (-66.1,-62.3)	-63.4 (-66.2,-60.9)	133	0.702
R_{input} (MΩ)	105.5 (62.8,133.9)	104.6 (72.0,138.8)	130	0.873	119.7 (98.1,145.4)	103.4 (80.5,123.5)	97	0.106
Tau (ms)	13.4 (9.4,18.4)	13.8 (9.1,15.2)	133	0.957	16.0 (12.8,17.9)	15.0 (12.4,19.3)	139	0.865
Sag (%)	7.9 (5.1,11.3)	4.4 (2.3,13.3)	110	0.381	3.5 (-2.7,7.6)	2.3 (-2.6,4.1)	122	0.454
Rheobase (pA)	109.5 (64.4,143.5)[a]	117.7 (85.1,171.9)[a]	99	0.444	99.4 (82.7,130.0)	137.6 (99.4,172.7)[a]	98	0.179
AP threshold (mV)	-38.7 (-44.1,-37.7)	-39.6 (-41.2,-38.3)	133	0.957	-36.6 (-39.0,-34.8)	-37.9 (-40.4,-35.4)	114	0.306
AHP (mV)	-2.8 (-8.6,-1.7)	-3.5 (-5.6,-1.4)	132	0.929	-6.4 (-8.5,-4.5)	-4.8 (-8.5,-1.9)	111	0.260
mAHP amplitude (mV)	-2.1 (-2.7,-1.1)[c]	-1.1 (-3.1,-0.5)[b]	83	0.720	-0.8 (-2.0,-0.4)	-1.1 (-2.3,-0.3)[a]	131	0.873
mAHP area (mV.ms)	-0.15 (-0.18,-0.07)[c]	-0.08 (-0.19,-0.03)[b]	80	0.616	-0.06 (-0.15,-0.02)	-0.09 (-0.19,-0.02)[a]	131	0.873
ADP presence (#cells)	8/18	9/15[b]	$\chi^2 = 0.79$	0.373	10/17	7/17	$\chi^2 = 1.06$	0.303
ADP amplitude (mV)	0.94 (0.32,1.70)	0.79 (0.12,1.56)	40	0.677	0.32 (1.13,1.03)	0.22 (0.04,1.02)	19	0.535
AP amplitude (mV)	67.9 (64.0,79.5)	68.9 (65.5,76.2)	134	0.986	65.2 (58.0,78.9)	69.6 (62.7,76.8)	131	0.658
AP half width (ms)	0.88 (0.80,0.98)	0.92 (0.75,1.01)	123	0.682	0.99 (0.91,1.07)	0.93 (0.85,1.00)	114	0.306
AP max RoR ($mV.ms^{-1}$)	271 (244,349)	266 (236,323)	131	0.901	238 (209,338)	269 (235,344)	117	0.357
		Factor	**F**	**P-value**		**Factor**	**F**	**P-value**
Cell firing	**Mixed-effects model**	Current	$F_{(1.2, 37.7)} = 144$	$<1x10^{-15}$	**Mixed-effects model**	Current	$F_{(1.5, 46.4)} = 424$	$<1x10^{-15}$
		Labelling	$F_{(1,31)} = 0.68$	0.41		Labelling	$F_{(1,32)} = 2.04$	0.16
		Interaction	$F_{(4,123)} = 0.58$	0.68		Interaction	$F_{(4,127)} = 1.6$	0.18

Table 4. Summary of physiological properties of layer 5 and 2/3 prefrontal cortex tdTom- and tdTom+ pyramidal neurons recorded from ex vivo slices from animals which underwent a second test phase (related to Fig. 3e,f). Values represent median (25,75 percentiles). Reported statistical values show Mann Whitney U test with 2-tailed p-value, except for ADP presence which uses Chi-squared test with 2-tailed p value. [a]*data not collected for 1 cell*. [b]*data not collected for 3 cells*. [c]*data not collected for 4 cells*. RMP resting membrane potential, R_{input} input resistance, AP action potential, AHP afterspike-hyperpolarisation, mAHP medium AHP, ADP afterspike-depolarisation, RoR rate of rise

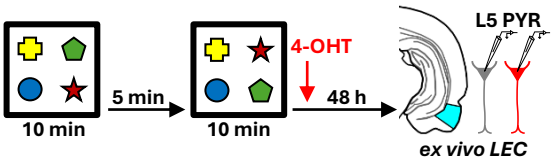

Physiological property	tdTom- L5 LEC pyramidal cells	tdTom+ L5 LEC pyramidal cells	Mann Whitney U	P-value
n (cells, mice)	21, 10	20, 10		
n cells (DLE, DIE, VIE)	19, 1, 1	18, 1, 1		
RMP (mV)	-62.8 (-65.0,-59.5)	-62.3 (-63.6,-58.0)	173.5	0.348
R_{input} (MΩ)	82.6 (68.6,127.0)	71.7 (53.3,111.6)	172	0.332
Tau (ms)	15.8 (12.9,21.2)	16.2 (13.6,19.4)	209	0.990
Sag (%)	12.6 (6.1,15.9)	10.9 (2.7,24.6)	201	0.826
Rheobase (pA)	126.7 (101.5,165.5)	152.7 (88.1,181.8)	190	0.615
AP threshold (mV)	-36.5 (-40.7,-32.5)	-38.4 (-42.9,-34.6)	158	0.181
AHP (mV)	-5.9 (-11.0,-4.1)	-5.6 (-8.8,-3.3)	180	0.446
mAHP amplitude (mV)	-1.8 (-2.9,-0.6)	-1.5 (-3.1,-0.5)	207	0.949
mAHP area (mV.ms)	-0.13 (-0.23,-0.03)	-0.11 (-0.24,-0.03)	203	0.867
ADP presence (#cells)	4/21	5/20	χ^2 = 0.21	0.645
ADP amplitude (mV)	0.60 (0.11,2.25)	0.35 (0.16,1.45)	8	0.730
AP amplitude (mV)	63.3 (59.7,69.2)	73.3 (62.6,80.7)	146	0.098
AP half width (ms)	0.92 (0.77,0.97)	0.84 (0.79,0.94)	195	0.703
AP max RoR ($mV.ms^{-1}$)	241 (212,322)	294 (252,381)	148	0.109
		Factor	**F**	**P-value**
Cell firing	**Mixed-effects model**	Current	$F_{(1.6, 60.35)}$ = 153	$<1x10^{-15}$
		Labelling	$F_{(1,39)}$ = 0.003	0.96
		Interaction	$F_{(4,156)}$ = 0.55	0.76

Table 5. Summary of physiological properties of layer 5 LEC tdTom- and tdTom+ neurons recorded from ex vivo slices from animals which did not undergo a second test phase (related to Fig. 4a). Values represent median (25,75 percentiles). Reported statistical values show Mann Whitney U test with 2-tailed p-value, except for ADP presence which uses Chi-squared test with 2-tailed p value. RMP resting membrane potential, R_{input} input resistance, AP action potential, AHP afterspike-hyperpolarisation, mAHP medium AHP, ADP afterspike-depolarisation, RoR rate of rise

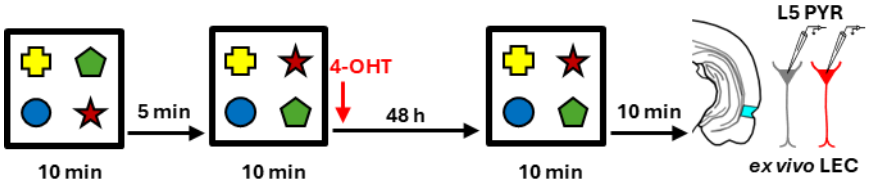

Physiological property	tdTom- L5 LEC pyramidal cells	tdTom+ L5 LEC pyramidal cells	Mann Whitney U	P-value
n (cells, mice)	31, 7	30, 7		
n cells (DLE, DIE, VIE)	29, 2, 0	28, 2, 0		
RMP (mV)	-65.3 (-67.9,-62.1)	-64.3 (-66.8,-62.7)	425.5	0.574
R_{input} (MΩ)	76.1 (56.0,102.3)	82.0 (56.3,99.6)	449	0.824
Tau (ms)	17.0 (13.6,19.6)	15.1 (12.2,19.6)	434	0.662
Sag (%)	11.7 (6.0,16.9)	10.3 (5.5,16.8)	454	0.881
Rheobase (pA)	144.2 (103.6,233.5)[a]	150.3 (90.40,207.8)	442	0.912
AP threshold (mV)	-39.4 (-41.8,-34.4)	-37.1 (-39.9,-33.6)	374	0.193
AHP (mV)	-7.3 (-10.8,-4.3)	-6.5 (-11.4,-5.1)	454	0.881
mAHP amplitude (mV)	-1.4 (-2.2,-0.8)[a]	-1.8 (-3.0,-0.8)[a]	389	0.493
mAHP area (mV.ms)	-0.11 (-0.17,-0.06)[a]	-0.12 (-0.23,-0.05)[a]	384	0.447
ADP presence (#cells)	4/30[a]	8/30	χ^2 = 1.67	0.197
ADP amplitude (mV)	0.12 (0.09,1.58)[a]	1.46 (0.45,1.86)	10	0.368
AP amplitude (mV)	72.0 (63.7,79.4)	67.1 (60.7,78.5)	369	0.170
AP half width (ms)	0.81 (0.78,0.91)	0.84 (0.75,0.90)	438	0.704
AP max RoR ($mV.ms^{-1}$)	304 (263,377)	269 (226,362)	388	0.272
Cell firing	**Mixed-effects model**	**Factor**	**F**	**P-value**
		Current	$F_{(1.3, 74.68)} = 156$	$<1x10^{-15}$
		Labelling	$F_{(1,59)} = 0.004$	0.85
		Interaction	$F_{(4,236)} = 0.34$	0.86

Table 6. Summary of physiological properties of layer 5 LEC tdTom- and tdTom+ neurons recorded from ex vivo slices from animals exposed to familiar object configuration at test 2 (related to Fig. 4b). Values represent median (25,75 percentiles). Reported statistical values show Mann Whitney U test with 2-tailed p-value, except for ADP presence which uses Chi-squared test with 2-tailed p value. [a]*data not collected for one cell*. RMP resting membrane potential, R_{input} input resistance, AP action potential, AHP afterspike-hyperpolarisation, mAHP medium AHP, ADP afterspike-depolarisation, RoR rate of rise.

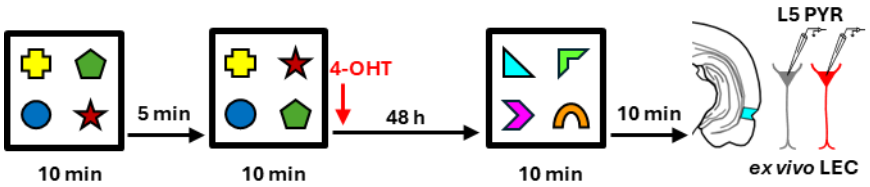

Physiological property	tdTom- L5 LEC pyramidal cells	tdTom+ L5 LEC pyramidal cells	Mann Whitney U	P-value
n (cells, mice)	31, 9	32, 9		
n cells (DLE, DIE, VIE)	29, 2, 0	29, 3, 0		
RMP (mV)	-63.2 (-64.9,-61.0)	-63.2 (-67.2,-58.1)	249.5	0.997
R_{input} (MΩ)	81.6 (62.6,102.8)	88.2 (57.9,125.2)	445	0.490
Tau (ms)	16.2 (12.7,18.3)	16.1 (13.8,18.0)	473	0.759
Sag (%)	14.6 (7.1,21.9)	11.86 (5.67, 17.77)	396	0.173
Rheobase (pA)	155.5 (120.1, 236.8)	156.3 (115.2,199.4)	442	0.465
AP threshold (mV)	-38.0 (-40.5,-35.8)	-36.4 (-39.9,-34.3)	378	0.107
AHP (mV)	-7.9 (-10.2,-4.5)	-6.3 (-8.1,-3.1)	391	0.152
mAHP amplitude (mV)	-2.3 (-3.7,-1.3)	-1.5 (-2.8,-0.8)	378	0.107
mAHP area (mV.ms)	-0.16 (-0.27,-0.10)	-0.12 (-0.21,-0.06)	389	0.144
ADP presence (#cells)	16/31	9/32	χ^2 = 1.91	0.057
ADP amplitude (mV)	0.48 (0.17,0.88)	0.38 (0.24,1.38)	71	0.978
AP amplitude (mV)	71.3 (63.4,78.4)	64.2 (55.4,73.4)	337	0.029
AP half width (ms)	0.79 (0.72,0.87)	0.88 (0.79,0.94)	289	0.004
AP max RoR ($mV.ms^{-1}$)	293 (240,373)	242 (200,302)	298.5	0.006
Cell firing	**Mixed-effects model**	**Factor**	**F**	**P-value**
		Current	$F_{(1.3, 81.67)}$ = 182	$<1x10^{-15}$
		Labelling	$F_{(1,61)}$ = 0.001	0.97
		Interaction	$F_{(4,244)}$ = 0.23	0.92

Table 7. Summary of physiological properties of layer 5 LEC tdTom- and tdTom+ neurons recorded from ex vivo slices from animals were exposed to a new object set prior to slice preparation (related to Fig. 4c). Values represent median (25,75 percentiles). Reported statistical values show Mann Whitney U test with 2-tailed p-value, except for ADP presence which uses Chi-squared test with 2-tailed p value. RMP resting membrane potential, R_{input} input resistance, AP action potential, AHP afterspike-hyperpolarisation, mAHP medium AHP, ADP afterspike-depolarisation, RoR rate of rise.

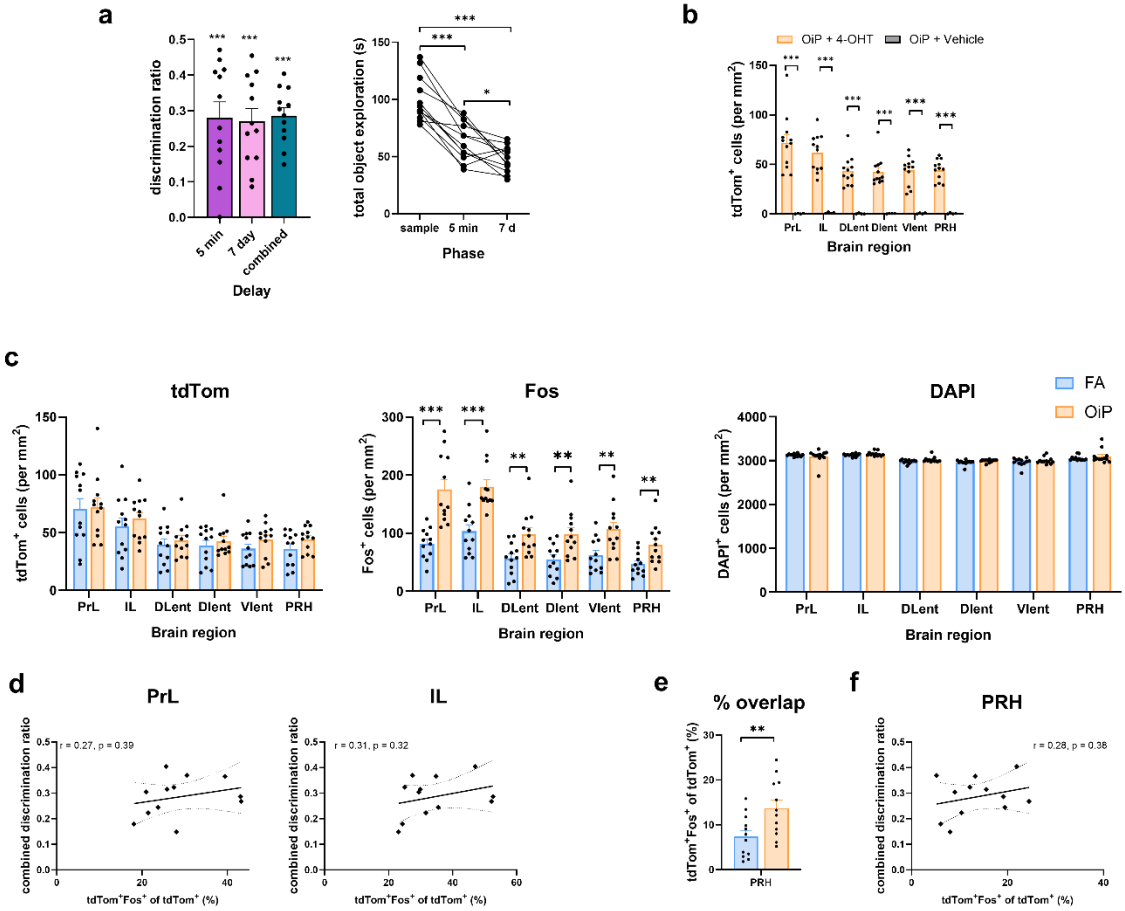

Supplementary Figure 1. Behavioural and labelling data from FA and OiP tasks.

a: (Left) Animals showed significant discrimination between the moved and unmoved objects in the OiP task, as measured by the discrimination ratio, at 5 min and 7 d delays and when combined (5 min $t_{(11)} = 7.55$, $p = 1.15 \times 10^{-5}$; 7 day $t_{(11)} = 6.31$, $p = 5.79 \times 10^{-5}$; combined $t_{(11)} = 12.79$, $p = 6.04 \times 10^{-8}$). (Right) Total object exploration significantly decreased across each phase of the behavioural task ($F_{(2,22)} = 46.99$, $p = 1.14 \times 10^{-8}$, post-hoc sample vs 5 min $p = 2.82 \times 10^{-5}$, sample vs 7 day: $p = 1.91 \times 10^{-5}$, 5 min vs 7 day: $p = 0.032$). **b**: Expression of tdTom was dependent on injection of 4-OHT in all brain regions (in each brain region one-way ANOVA $F_{(1,14)} > 28$, $p < 0.001$). OiP + 4-OHT n = 12, OiP + vehicle n = 4. **c**: tdTom, Fos and DAPI cell counts in subregions of mPFC and LEC and in PRH for FA and OiP conditions. **d**: No significant correlation between tdTom and Fos overlap and memory performance in either PrL or IL subregions of mPFC. Dashed line show 95% confidence intervals. **e**: Overlap between tdTom and Fos

expression in the perirhinal cortex is significantly higher in the OiP compared to the FA condition. **f**: No significant correlation between tdTom and Fos overlap and memory performance in the perirhinal cortex. Dashed line show 95% confidence intervals. All bar charts show mean ± SEM. * $p < 0.05$, ** $p < 0.01$, *** $p < 0.001$. For FA vs OiP comparisons n = 12 animals for each condition. See Supplementary Data Table 1 for detailed statistical analysis.

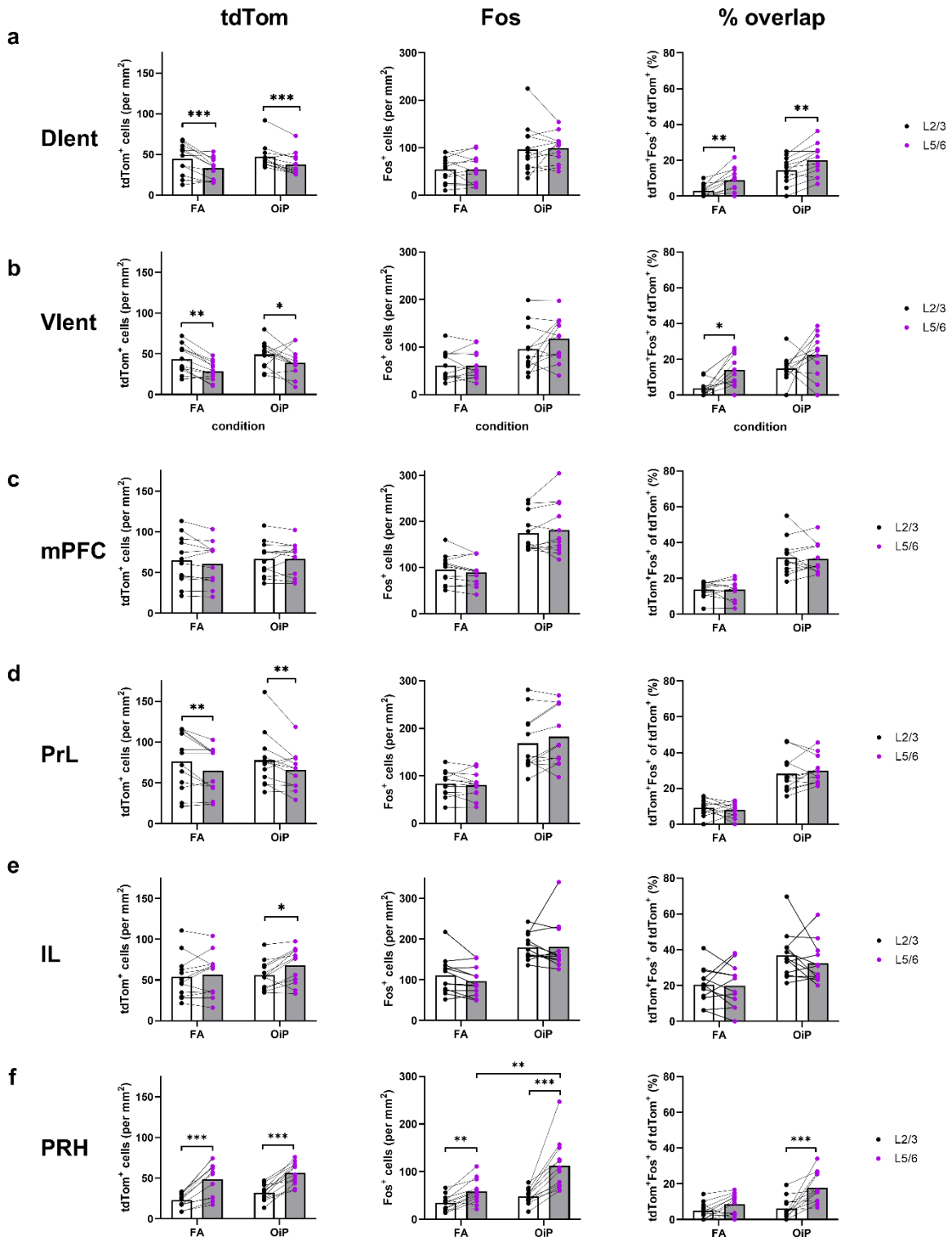

Supplementary Figure 2. Expression patterns of tdTom, Fos and overlap in layer 2/3 and layer 5/6 across cortical regions. a: (Left to right) tdTom, Fos and percent overlap for L2/3 and L5/6 in DIent. **b**: Same as (**a**) but for VIent. **c**: Same as (**a**) but for mPFC. **d**: Same as (**a**) but for PrL. **e**:Same as (**a**) but for IL. **f**: Same as (**a**) but for PRH. Bars represent mean values. *** p <

0.001, ** p < 0.01, * p < 0.05. n = 12 mice per condition. See Supplementary Data Table 2 for detailed statistical analysis.

Brain region	tdTom +ve cells		Fos +ve cells		% Overlap	
	$F_{(1,22)}$	P-value	$F_{(1,22)}$	P-value	$F_{(1,22)}$	P-value
mPFC	0.17	0.686	26.90	3.35×10^{-5}	38.54	3.01×10^{-6}
PrL	0.01	0.909	24.88	5.42×10^{-5}	58.95	1.16×10^{-7}
IL	0.55	0.466	21.20	1.38×10^{-4}	11.78	0.002
LEC	0.89	0.356	10.33	0.004	37.42	3.71×10^{-6}
DLent	0.40	0.534	9.40	0.006	26.26	3.90×10^{-5}
DIent	0.39	0.537	9.83	0.005	20.59	1.62×10^{-4}
VIent	2.01	0.171	9.33	0.006	27.62	2.85×10^{-5}
PRH	2.60	0.121	9.26	0.006	7.64	0.011

Supplementary Data Table 1: Statistical analysis of tdTom and Fos expression and % overlap across mPFC and LEC (and subdivisions) and PRH. Data shows outcome of one-way ANOVA with behavioural task as a between subjects factor. For both conditions n = 12 mice.

Brain region	Factor	tdTom +ve cells		Fos +ve cells		% overlap	
		$F_{(1,22)}$	P-value	$F_{(1,22)}$	P-value	$F_{(1,22)}$	P-value
mPFC	Behaviour	0.17	0.686	26.90	3.35×10^{-5}	39.22	3.0×10^{-6}
	Depth	1.28	0.270	0.02	0.877	0.09	0.770
	Interaction	1.43	0.244	3.03	0.096	0.07	0.790
PrL	Behaviour	0.01	0.909	24.88	5.42×10^{-5}	61.68	8.01×10^{-8}
	Depth	13.70	0.001	3.79	0.064	0.30	0.864
	Interaction	0.01	0.929	1.85	0.188	1.76	0.198
IL	Behaviour	0.55	0.466	21.20	1.38×10^{-4}	11.97	0.002
	Depth	7.99	0.010	0.96	0.338	1.09	0.308
	Interaction	2.85	0.106	1.17	0.291	0.76	0.394
LEC	Behaviour	0.89	0.356	10.33	0.004	32.75	9.34×10^{-6}
	Depth	49.40	4.72×10^{-7}	0.14	0.712	50.08	4.25×10^{-7}
	Interaction	1.36	0.256	0.86	0.364	0.01	0.928
DLent	Behaviour	0.40	0.534	9.40	0.006	22.97	8.71×10^{-5}
	Depth	5.59	0.027	1.52	0.231	26.18	4.04×10^{-5}
	Interaction	0.27	0.606	0.04	0.847	0.03	0.870
DIent	Behaviour	0.39	0.537	9.83	0.005	18.21	3.14×10^{-4}
	Depth	33.08	8.72×10^{-6}	0.05	0.819	34.18	7.00×10^{-6}
	Interaction	0.39	0.539	0.04	0.853	0.01	0.945
VIent	Behaviour	2.01	0.171	9.33	0.006	16.81	4.72×10^{-4}
	Depth	15.96	6.11×10^{-4}	2.55	0.125	11.25	0.003
	Interaction	0.55	0.467	2.55	0.125	0.31	0.583
PRH	Behaviour	2.60	0.121	9.26	0.006	6.94	0.015
	Depth	99.59	1.25×10^{-9}	40.84	1.98×10^{-6}	21.03	1.44×10^{-4}
	Interaction	0.14	0.717	866	0.008	5.56	0.028

Supplementary Data Table 2: Statistical analysis of tdTom and Fos expression and % overlap in superficial and deep layers of PFC, LEC and PRH. Data shows outcome of two-way ANOVA with behavioural condition (beh. cond.) as a between-subjects factor and depth as a within-subjects factor. n = 12 mice per condition.